

Journal Pre-proof

Acoustic scattering characteristics and inversions for suspended concentration and particle size above mixed sand and mud beds

Peter D. Thorne, Ian D. Lichtman, David Hurther



PII: S0278-4343(20)30273-9

DOI: <https://doi.org/10.1016/j.csr.2020.104320>

Reference: CSR 104320

To appear in: *Continental Shelf Research*

Received Date: 12 June 2020

Revised Date: 21 November 2020

Accepted Date: 27 November 2020

Please cite this article as: Thorne, P.D., Lichtman, I.D., Hurther, D., Acoustic scattering characteristics and inversions for suspended concentration and particle size above mixed sand and mud beds, *Continental Shelf Research* (2020), doi: <https://doi.org/10.1016/j.csr.2020.104320>.

This is a PDF file of an article that has undergone enhancements after acceptance, such as the addition of a cover page and metadata, and formatting for readability, but it is not yet the definitive version of record. This version will undergo additional copyediting, typesetting and review before it is published in its final form, but we are providing this version to give early visibility of the article. Please note that, during the production process, errors may be discovered which could affect the content, and all legal disclaimers that apply to the journal pertain.

© 2020 Published by Elsevier Ltd.

1 N:\My-Documents\docw7\2020\mixed-sed\Thorne-muddysand-resubmitted2.docx

2

3 **Acoustic scattering characteristics and inversions for suspended**
4 **concentration and particle size above mixed sand and mud beds**

5

6

7 Peter D. Thorne^{1*}, Ian D. Lichtman¹ and David Hurther²

8

9 1. National Oceanography Centre, Joseph Proudman Building, 6 Brownlow Street, Liverpool,
10 L3 5DA, United Kingdom.

11 2. Laboratory of Geophysical and Industrial Flows (LEGI), CNRS, University Grenoble
12 Alpes, Grenoble-INP, France

13

14 *Corresponding author. Email: pdt@noc.ac.uk, Tel: +44 151 795 4862

15 21/11/2020

16

17

Abstract

18

19 The majority of reported field studies, using acoustic backscattering, for the measurement of
20 nearbed suspended sediment processes, have been focussed on field sites with sand size
21 fractions and unimodal size distributions. However, in many sedimentary environments, and
22 particularly for estuaries and rivers, sands and muds coexist in the bed sediment substrate,
23 forming a size regime that is often bimodal in nature. To examine the interaction of sound in
24 these more complex sedimentary environments a numerical study is presented based on
25 observations of sediment size distributions measured in the Dee estuary, UK. The work
26 explores the interpretation of the backscatter signal from a mixed sediment composition in
27 suspension, with mud-sand fractions varying with height above the bed. Consideration is
28 given to the acoustical scattering properties and the inversion of the backscatter signal to
29 extract information on the suspension. In common with most field deployments, the scenarios
30 presented here use local bed sediments for the acoustic inversion of the backscattered signal.
31 The results indicate that in general it is expected that particle size and concentration will
32 diverge from what is actually in suspension, with the former being overestimated and the
33 latter underestimated.

34

35 Key words: Acoustics, sediments, scattering, modelling, suspensions, inversion

36

37

1. Introduction

38 Developments in the application of acoustics, to the measurement of sediment transport
39 processes, is an ongoing area of research (Thorne et al., 2018). It is within this context that
40 the present study examines its application to the measurement of suspended sediments, above
41 a bed of mixed composition. In general the deployment of acoustic backscatter systems, ABS,
42 in coastal environments, for sediment transport process studies, has been under conditions
43 where the suspensions were considered to be in the sand regime, with a unimodal size
44 distribution (Young et al., 1982; Vincent et al., 1982; Hanes et al., 1988; Lynch et al., 1991;
45 Hay and Sheng 1992; Crawford and Hay 1993; Thorne et al., 1993; Lynch et al., 1994;
46 Osborne and Vincent 1996; Thorne and Hardcastle 1997; Villard et al., 2000; Thorne et al.,
47 2002; Cacchione et al., 2008, O'Hara Murray et al., 2011; Moate et al., 2015). However, in
48 many marine environments, particularly estuaries and rivers, the composition of sediments is
49 more complex, often with mixtures of sands and muds with a bimodal size distribution.
50 Therefore, the deployment of ABS and the interpretation of the backscattered signal in such
51 environments is of interest. In the study presented here, consideration is given to the impact
52 upon acoustics backscattering and attenuation, of having a very broad bimodal mass size
53 distribution, in which particles span the size range from sub-micron clays, to hundreds of
54 microns sands. The interest in looking at this scenario is associated with some recent
55 measurements of bed sediments and suspended sediments, collected over a muddy sand bed
56 in an inter-tidal estuarine environment (Lichtman et al., 2018). The composition of the
57 suspended sediments changed significantly with height above the bed and this has
58 implications for the interpretation of the acoustic backscattered signal and suspended
59 sediment estimates. To address this problem a numerical study is presented, which aims to
60 examine in a practical manner, the implications for acoustic measurements of suspended
61 sediments in a mixed sediment environment.

62

63 To underpin this study, use is made of the laboratory and theoretical studies conducted to
64 provide a framework for understanding the interaction of sound with suspended sediments
65 and for inverting the backscatter signal to obtain suspension parameters. Measurements of the
66 backscatter characteristics of aqueous suspensions, often expressed non-dimensionally using
67 the form function (Sheng and Hay, 1988; Thorne et al., 1993) have been carried out over the
68 past three decades (Hay, 1991; He and Hay, 1993; Thorne and Buckingham, 2004; Moate and

69 Thorne, 2012) leading to a number of comparable expressions. Similarly, the scattering
70 attenuation can be represented non-dimensionally using the normalised total scattering cross-
71 section (Flammer, 1962; Schaafsma and Hay 1997; Thorne and Buckingham, 2004; Moate
72 and Thorne, 2009) with again a number of similar expressions representing the observations.
73 Most of these works were collected together in Thorne and Meral (2008). Studies have also
74 looked at sediments of different and mixed mineralogy (Moate and Thorne, 2012), the
75 angular scattering characteristics of suspension (Moore and Hay, 2009) and visco-thermal
76 attenuation by suspended particles (Urlick, 1948; Hay and Mercer, 1985; Richards et al.,
77 2003; Moore et al., 2013). In these studies, the suspensions generally consisted of unimodal
78 relatively narrow sized suspensions.

79

80 To utilise the above laboratory and theoretical studies in field deployments of ABS, requires
81 a description of the size distribution of the suspension, to enable calculation of the scattering
82 characteristics. In most marine studies, in-situ detailed measurements of suspended sediment
83 size distribution are unavailable. The general approach has therefore been to collect bed
84 sediments when possible (Hay and Sheng, 1992; Thorne et al., 1993; Osborne and Vincent,
85 1996; Thorne and Hardcastle, 1997; Lee et al., 2004; Bolanos et al., 2012; Moate et al., 2016)
86 and obtain a mass size distribution by using a stack of $\frac{1}{4} \phi$ sieves, $\phi = -\log_2(d)$ where d is the
87 particle diameter in mm (Soulsby 1997). Such an approach preferentially samples the sand
88 size component of the distribution, particularly if only a small proportion of the bed
89 sediments are in the muddy regime. For a calibrated ABS system as described in Betteridge et
90 al., 2008, the sieved size distribution would be used for acoustic inversions. Alternatively, the
91 ABS could be site specific calibrated using the bed sediments. Using either approach,
92 inversions are based on bed sediment samples. In the present study, a numerical analysis is
93 carried out to assess the impact of using bed sediment samples, for acoustic estimates of
94 suspended mean particle size and concentration, under conditions of varying suspension
95 composition with height above the bed. The analysis is conducted under conditions of sandy
96 sediments dominating the mass concentration near the bed and muddy sediments becoming
97 more predominate with height above the bed. Given the broadening use of acoustics in more
98 complex sedimentary environments (Shi et al., 1996, 1997; Holdaway 1999, Bartholoma et
99 al., 2009; Sassi et al., 2012, 2013; Moore et al., 2012, 2013; Guerrero et al, 2013;
100 Dwinovantyo et al., 2017; Fromant et al., 2017; Vergne et al., 2020), it was considered such a

101 study would be timely and of use to the coastal, riverine and estuarine communities using
102 acoustics for suspended sediment studies in mixed sedimentary environments.

Journal Pre-proof

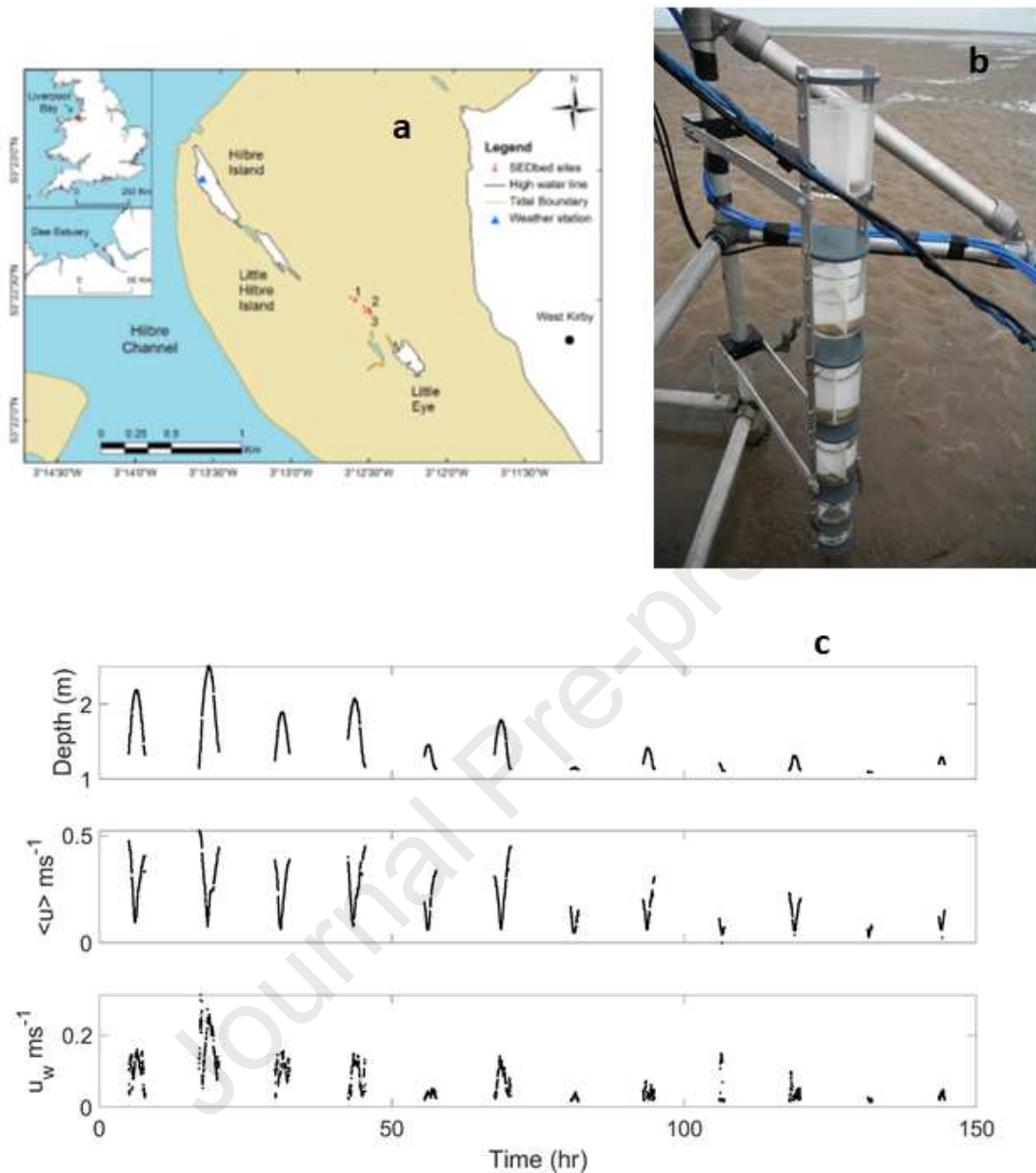
103

2. Measurements of particle size distribution.

104 Hydrodynamic and sediment process data, were collected on an intertidal flat in the Dee
105 estuary, located on the north west coast of the UK, as part of studies on ripple migration and
106 bed material transport rates in mixed muddy sands (Lichtman et al., 2018). The estuary is
107 tidally dominated, with a 7-8 m mean spring tidal range and data were collected in early
108 summer over a spring-neap cycle, in order to cover various mixtures of sand and mud
109 composition. As part of the study, surficial sediment samples from the bed were collected at
110 low tide when the bed sediments were exposed. Suspended sediment samples were obtained
111 during periods of tidal inundation, using a novel multi-tier cylinder unit. Figure 1, shows the
112 site location, a photograph of the unit and an overview of the hydrodynamics. The individual
113 cylinders had a height and diameter of 0.1m and 0.09 m respectively and were located at 0.2,
114 0.41, 0.58, 0.74 and 1.0 m above the bed. The cylinders obtained samples of the suspended
115 sediments, transported by currents and waves, as they descended towards the bed under
116 gravity. To reduce turbulence within the cylinders of the tier and possible resuspension of the
117 collected sediments, baffles were installed within the cylinders. The multi-tier sampler,
118 cumulatively collected suspended sediments over several tidal inundations, under changing
119 hydrological conditions. These samples were recovered at the end of the 150 hr measurement
120 period and are considered to be indicative of the average suspended sediments size
121 distributions, at the field site, over the deployment period. The size distributions of the bed
122 and multi-tier sediments were measured over the size range $1.10^{-7} - 2.10^{-3}$ m, using a
123 Malvern Mastersizer 2000, a laboratory laser diffraction particle size analyser. The
124 Mastersizer rather than sediment sieving was used to ensure any fine muddy components of
125 the bed and suspended sediments were captured in the size analysis. Since the finer particles
126 may have adhered to one other as settling occurred in the tiers, the sediment samples were
127 dispersed to ensure it was the primary particle size distribution that was being measured.

128

129



130

131

132 Fig 1. a) Site location, 1-3, in the Dee Estuary, UK. b) Photograph of the multi-tier cylinder
 133 unit used to capture suspended sediments, above a bed of muddy sand. c) Measurements of
 134 the water depth, depth averaged velocity, $\langle u \rangle$ and wave orbital velocity, u_w .

135

136 2.1 Bed sediments

137 Figure 2a shows the mass concentration size probability density distribution, $P_b^c(a)$, for the
 138 bed, a is the particle radius. This shows the bed sediments to be dominated by sand with a

139 small muddy component indicated by the low values between $a=0.5-30 \mu\text{m}$. Mud is defined
 140 on the Wentworth scale (Whitehouse et al., 2000) as a mixture of mainly fine-grained
 141 sediments (clays and silt) with diameters less than $63 \mu\text{m}$. In most nearbed sediment process
 142 field studies only bed samples are available for aiding the analysis of the acoustic backscatter
 143 data, due to the difficulties of collecting time series of in-situ suspended sediment samples.
 144 Bed samples are therefore generally used to carryout post-deployment laboratory ABS
 145 calibration, or, by measuring the size distribution, carrying out a more theoretical inversion
 146 (Hanes, 1991; Hay and Sheng, 1992; Osborne and Vincent, 1996; Green and Black 1999; Lee
 147 et al., 2004; Bolanos et al., 2012; Moate et al., 2016). Given the dominance of the sandy
 148 component in figure 2a it would seem reasonable to fit a probability density function to the
 149 sandy component for interpretation of the backscatter signal. A lognormal probability density
 150 function was fitted to the bed data, and as can be seen in figure 2a, there is good agreement
 151 between this fit and the measurements. The lognormal distribution is given by:

152

$$P_b^c(a) = \frac{1}{a\zeta\sqrt{2\pi}} e^{-(\ln(a)-\gamma)^2/2\zeta^2} \quad (1)$$

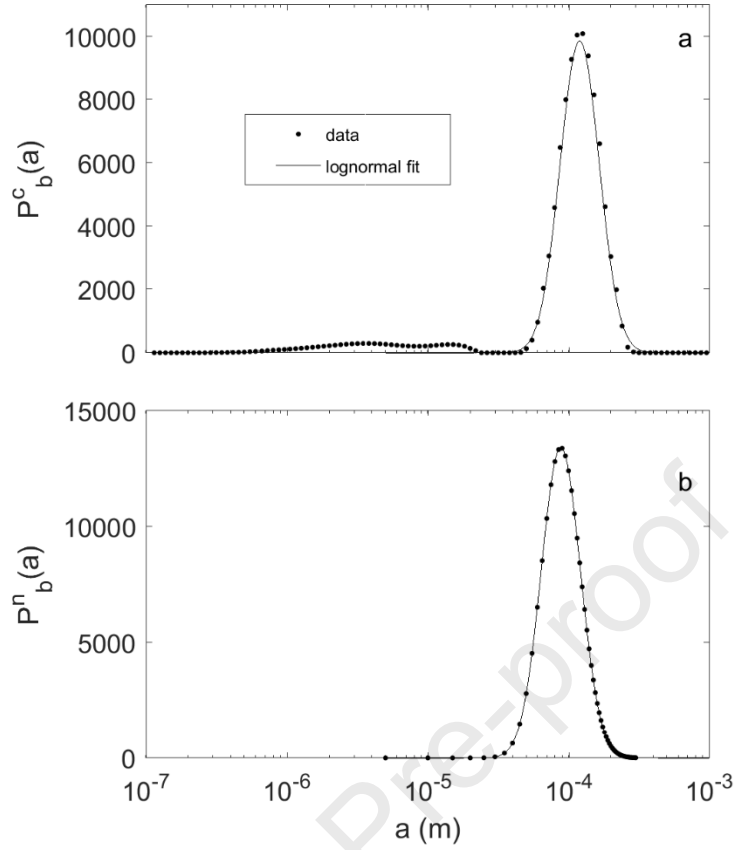
153

$$\zeta = \sqrt{\ln[(\sigma_{cb}/a_{cb})^2 + 1]},$$

$$\gamma = \ln(a_{cb}^2/\sqrt{a_{cb}^2 + \sigma_{cb}^2})$$

154

155 Where the subscript 'b' refers to the bed and 'c' mass concentration. For the distribution a_{cb} is
 156 the mean radius and σ_{cb} the standard deviation, these had values respectively of $140 \mu\text{m}$ and
 157 $46 \mu\text{m}$.



158

159

160 Fig 2. a) Comparison a lognormal distribution $P_b^c(a)$ (—) with the measured concentration
 161 radius probability distribution of the bed sediments, (•) and b) comparison a lognormal
 162 distribution $P_b^n(a)$ (—), with the number radius probability distribution, calculated using
 163 equation (2), with the fitted lognormal distribution to $P_b^c(a)$ (•).

164

165 For the analysis of acoustic backscatter data, it is the particle number size distribution, $P_b^n(a)$,
 166 which is required. This can be calculated for the bed, $z=0$, and the suspension, from $P_j^c(a, z)$,
 167 where z is the height above the bed, using:

168

$$P_j^n(a, z) = \frac{P_j^c(a, z)}{a^3(z)} / \left(\int_{a_1}^{a_2} \frac{P_j^c(a, z)}{a^3(z)} da \right) \quad (2)$$

169 Which has the condition,

$$\int_{a_1}^{a_2} P_j^n(a, z) da = 1$$

170 Here a_1 and a_2 are the lower and upper values of the size distribution and $j=b$ or s to represent
 171 the bed or the suspension. The evaluation of equation (2) using a lognormal distribution for
 172 $P_b^c(a)$ at $z=0$, results in a lognormal distribution for $P_b^n(a)$, with a smaller value for the mean
 173 number radius, $a_{nb}=103 \mu\text{m}$, while retaining the same σ_{nb}/a_{nb} ratio as for $P_b^c(a)$. This can be
 174 clearly seen in figure 2b. To obtain profiles of suspended sediment size and concentration
 175 from an inversion of multi-frequency acoustic backscatter data, requires a description for the
 176 form of $P_s^n(a, z)$. Given the lognormal fit to $P_b^c(a)$ for the bed sediments shown in figure 2a,
 177 and the lognormal fit to $P_b^n(a)$ as illustrated in figure 2b, it would not seem unreasonable to
 178 use the lognormal distribution of $P_b^n(a)$ for acoustics inversions, in the absence of
 179 independent suspended sediment measurements.

180

181 2.2 Suspended sediments

182 As described earlier, a novel multi-tier cylinder sampler was used to collect suspended
 183 sediments in the field, over several tidal cycles, to provide measurements of the particle mass
 184 size distribution with height above the bed, $P_s^c(a, z)$. The results from these measurements are
 185 shown in figure 3. Figure 3a shows the form of $P_s^c(a, z)$ at increasing heights above the bed.
 186 As can be observed the measured size range is from the sub-micron to near millimetric. The
 187 vertical line at $a=31.5 \mu\text{m}$ represents the demarcation between the mud and sand components.
 188 The plot shows an increasing mud content in the suspended sediments, with height above the
 189 bed. The mean mass concentration radius, $a_c(z)$, reduces from $140 \mu\text{m}$ at the bed, to $116 \mu\text{m}$
 190 at 1.0 m above the bed. The suspended sediments values for $P_s^c(a, z)$ have been converted to
 191 $P_s^n(a, z)$ using equation (2) and the results are shown in figure 3b. As can be seen the form for
 192 $P_s^n(a, z)$ is very different from $P_s^c(a, z)$, with $P_s^n(a, z)$ having a decreasing power law
 193 distribution with particle size and with the muddy component orders of magnitude greater
 194 than the sandy. The power law distribution for $P_s^n(a, z)$ is not uncommon in the marine
 195 environment in oceanic and estuarine waters (Babin, et al., 2003; Kostadinov et al., 2009;
 196 Buonassissi and Dierssen, 2010) and is generally referred to as the Junge distribution (Junge,
 197 1963). The form of a Junge distribution is shown by the dashed line with the measured values
 198 of $P_s^n(a, z)$ in figure 3b and has the simple form:

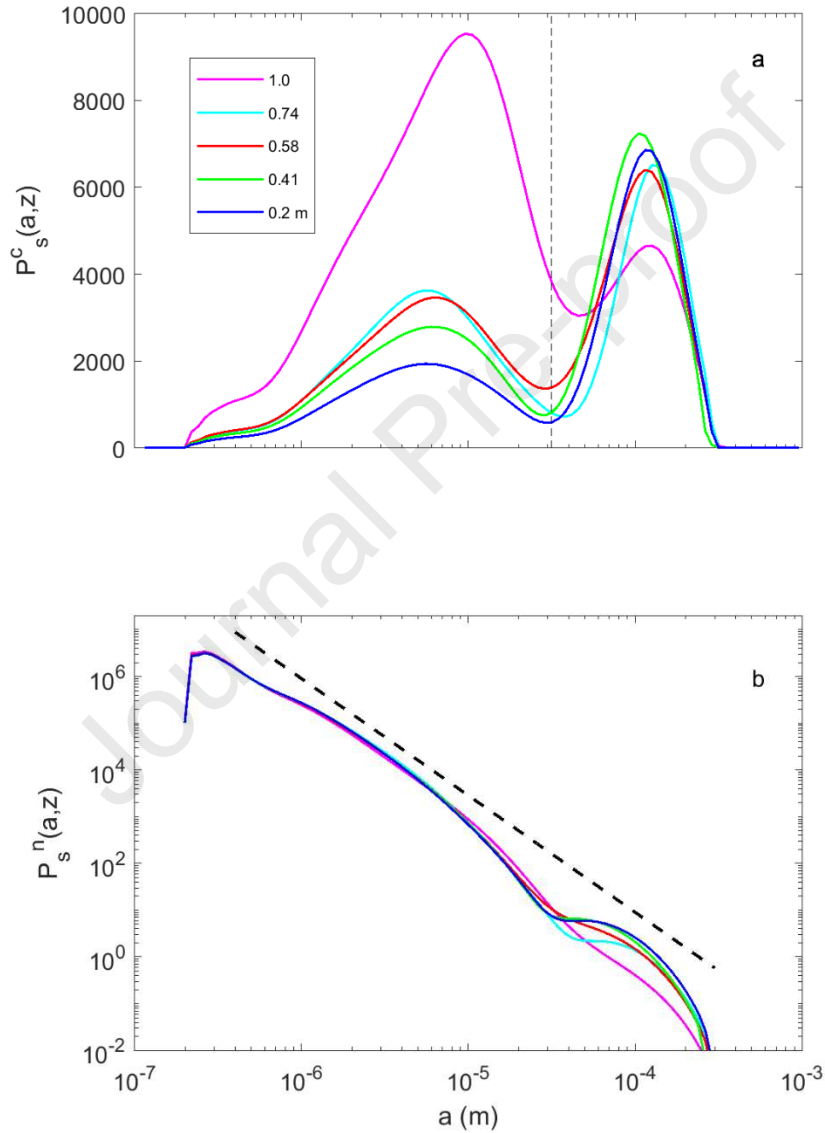
199

$$P_s^n(a) = N_0 a^{-J} \quad (3)$$

200

201 With $N_0=9 \cdot 10^{10}$ and $J=2.5$ where N_0 is a scaling parameter and J the slope of the distribution.

202



203

204 Fig 3. Measurements of the suspended sediments radius probability distributions for; a) the
 205 concentration, $P_s^c(a,z)$, showing an increasing mud ($a < 31.5 \mu\text{m}$, indicted by the dashed
 206 vertical line) and decreasing sand content with height above the bed, z , and b) the particle
 207 number, $P_s^n(a,z)$, calculated with equation (2) using $P_s^c(a,z)$. The legend provides the values of

208 z for the individual suspension curves. A Junge distribution (— —) is also shown for
209 comparison.

210

211 This Junge distribution is not intended to be a fit to the measurements, just simply to illustrate
212 the approximate power law form of the suspended number size distribution in the Dee
213 estuary. The mean number radius, $a_n(z)$, is almost uniform for the suspended sediments
214 reducing from $0.85 \mu\text{m}$ at 0.2 m above the bed to $0.78 \mu\text{m}$ at 1.0 m above the bed. The value
215 for $a_n(z)$ is therefore greater than two orders of magnitude smaller than $a_c(z)$.

216

217 Following the aims of the present study, it was considered of value to conduct an examination
218 of how an acoustic inversion, based on a lognormal fit to a bed particle number size
219 distribution, $P_b^n(a)$, such as in figure 2b, would impact on computed profiles of suspended
220 size and concentration, having number size distributions $P_s^n(a,z)$, closer to those shown in
221 figure 3b. Therefore, a case study is presented, based on the observations of the size
222 distributions measured in the Dee estuary, which explores the outcome of using a sandy bed
223 sediment size distribution, to interpret backscatter signals from a mixed composition in
224 suspension, with varying mud-sand fractions with height above the bed. This was carried out
225 as a numerical study, as there are no field or laboratory data available, with the detailed in-
226 situ suspended sediment measurements required to assess such an inversion. It was
227 considered such a study would provide some useful insights into the analysis of acoustic
228 backscatter data, collected above beds composed of mixed sediments, under hydrodynamic
229 conditions that lead to significant size sorting with height above the bed.

230

231 **3. Sediment size distributions and scattering characteristics.**

232

233 *3.1 Bed and suspended sediment size distributions.*

234 To carry out the study, mass size distributions were set up for the bed and suspended
 235 sediments which were comparable to those shown in figures 2 and 3. The bed sediments were
 236 represented by a lognormal distribution composed of medium sand:

$$P_b^c(a) = \frac{1}{a\zeta\sqrt{2\pi}} e^{-(\ln(a)-\gamma)^2/2\zeta^2} \quad (4a)$$

237

238 For the bed $a_{cb}=150 \mu\text{m}$ and $\sigma_{cb}/a_{cb}=0.3$ which is comparable to the values for the lognormal
 239 distribution in figure 2a. The suspended sediments were formed by combining two lognormal
 240 distributions as below:

241

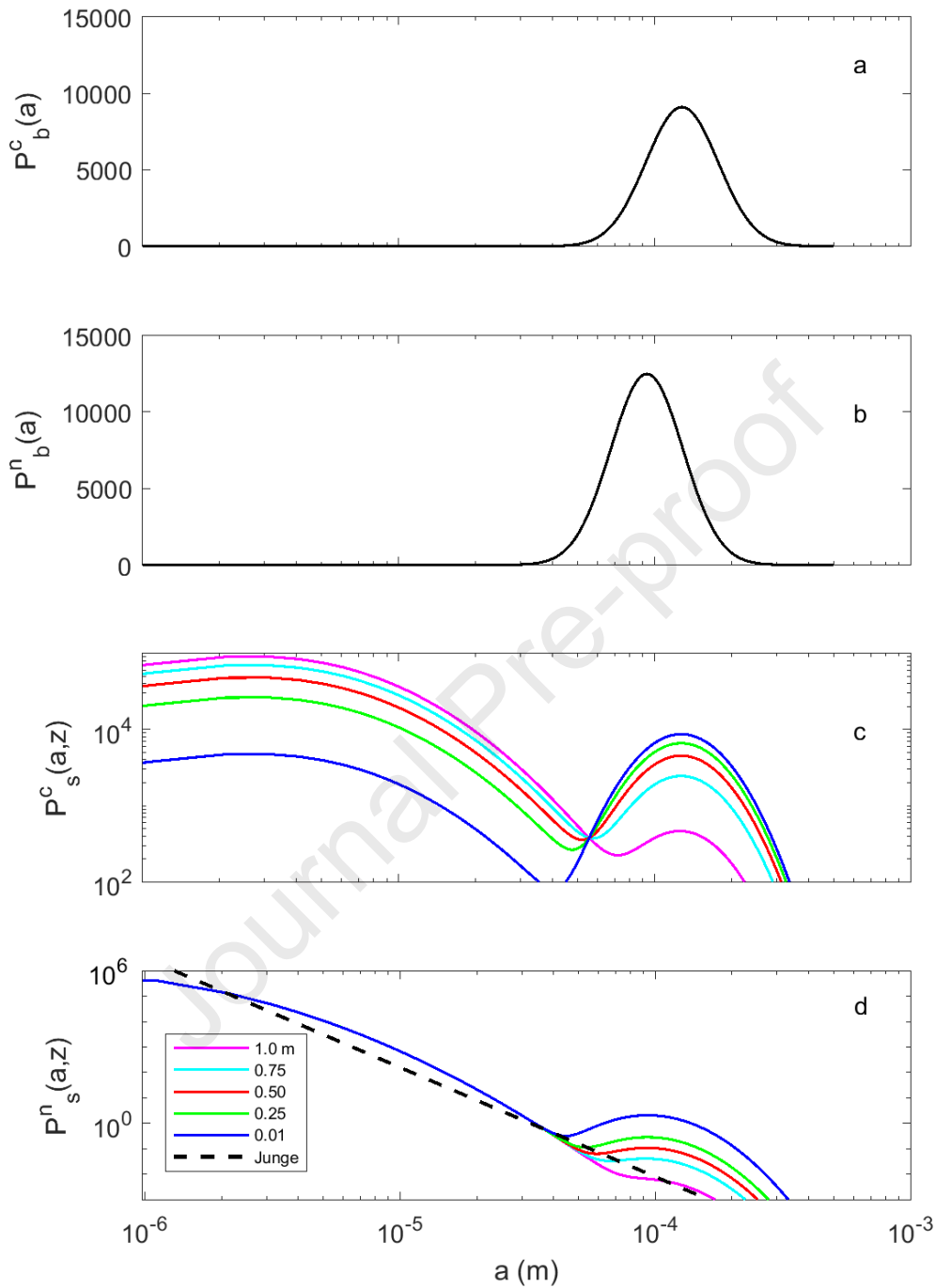
$$P_s^c(a, z) = \theta(z)P_b^c(a) + \frac{1 - \theta(z)}{a\zeta\sqrt{2\pi}} e^{-(\ln(a)-\gamma)^2/2\zeta^2} \quad (4b)$$

242

243 The second term in equation (4b), represents the suspended muddy component. This had a
 244 mean radius, a_{cu} , and standard deviation, σ_{cu} , of $a_{cu}=10 \mu\text{m}$ and $\sigma_{cu}/a_{cu}=1$. To characterize the
 245 suspended sediment mixture, $\theta(z)=0.95-0.05$ in one hundred equal intervals of 0.0091
 246 between $z=0.01-1.0$ m with 0.01 m spacing. This represents suspended sediment mass
 247 transitioning from 95% sand at 0.01 m above the bed to 95% mud at 1.0 m above the bed.
 248 The modelled suspension structure was selected to be bi-modal with reducing sand content
 249 with z to reflect the observations shown in figure 3a, rather than trying to replicate
 250 specifically the field parameters. In practice the functional form for $\theta(z)$ will depend on the
 251 hydrodynamics and site specific sediment composition, which could readily result in a more
 252 complex form for $\theta(z)$, than the linear model adopted for simplicity in the present study, to
 253 highlight compositional impacts. Plots of $P_b^c(a)$ and $P_s^c(a, z)$ are given respectively in figures
 254 4a and 4c. For the acoustic analysis $P_b^n(a)$ and $P_s^n(a, z)$ were required and these were obtained
 255 using equation (2).

256

257



258

259 Fig 4. Concentration and number size probability density distributions for; a) the bed, $P_b^c(a)$
 260 and b) $P_b^n(a)$ and for the suspended sediments c) $P_s^c(a,z)$ and d) $P_s^n(a,z)$. A Junge (— —)
 261 probability distribution function is also shown in d). The legend provides the values of z for
 262 the individual suspension curves.

263

264 The forms for these two distributions are shown in figure 4b and 4d and they are similar to
265 those in figures 2b and 3b. The lognormal distribution in figure 4b has a mean number size of
266 $a_{nb}=109 \mu\text{m}$ and $\sigma_{nb}/a_{nb}=0.3$. A Junge distribution is also shown for comparative purposes in
267 figure 4d. The profiles of the mean mass radius, $a_c(z)$, from figure 4c and mean number
268 radius, $a_n(z)$, from figure 4d are shown in figure 7. It can be seen in figure 7 that $a_c(z)$ shows a
269 steady decrease in size with z , while $a_n(z)$ is uniform and significantly smaller than $a_c(z)$, both
270 of which are consistent with the field observations.

271

272 Although in the marine environment flocculation may occur in the finer fraction of the size
273 distribution, this process and the associated acoustic scattering characteristics (MacDonald et
274 al., 2012; Thorne et al., 2014; Fromant et al., 2017) are not considered here. The distributions
275 in figure 4 represent the bed and suspended sediments distributions upon which the present
276 study is focussed.

277

278 *3.2 Acoustic scattering characteristics of the sediment distributions.*

279 The acoustic scattering properties of a suspension of sediments are normally described in
280 terms of the intrinsic scattering properties of the individually sized particles integrated over
281 the particle number size probability density distribution (Hay, 1991; He and Hay, 1993;
282 Thorne and Buckingham, 2004; Moate and Thorne, 2012). The intrinsic scattering
283 characteristics are represented by the backscatter form function, f_i and the normalised total
284 scattering cross-section, χ_i . Intrinsic refers to the scattering characteristics measured using
285 suspensions sieved into narrow $\frac{1}{4} \phi$ size fractions which provide a nominally single particle
286 size. Physically, f_i describes the backscattering characteristics of a particle relative to its
287 geometrical size, whilst χ_i quantifies the scattering from a particle over all angles, relative to
288 its cross-sectional area, and is proportional to scattering attenuation. Both parameters are
289 dimensionless. There are a number of similar expressions for f_i and χ_i (Sheng and Hay 1988;
290 Crawford and Hay, 1993; Thorne and Meral, 2008, Moate and Thorne 2012). Here use is
291 made of the expressions of Thorne and Meral (2008), based on a series of published data sets,
292 on acoustic scattering by narrowly sieved suspended sediments:

293

$$f_i(x) = \frac{(1 - 0.35e^{-((x-1.5)/0.7)^2})(1 + 0.5e^{-((x-1.8)/2.2)^2})x^2}{1 + 0.9x^2} \quad (5a)$$

294

$$\chi_i(x) = \frac{0.29x^4}{0.95 + 1.28x^2 + 0.25x^4} \quad (5b)$$

295

296 In equation (5), $x=2\pi af/c$, with f and c respectively the frequency and velocity of sound in the
 297 fluid and a is the particle radius. Owing to the inclusion of mud and sand components in the
 298 suspension to be studied, the finer fractions will introduce viscous attenuation. The
 299 normalised total viscous attenuation, χ_v , can be expressed as:

300

$$\chi_v = \frac{2}{3}x(\delta - 1)^2 \frac{\tau}{\tau^2 + (\delta + \varepsilon)^2} \quad (5c)$$

301

302 Where,

$$\tau = \frac{9}{4\beta a} \left(1 + \frac{1}{\beta a}\right), \quad \varepsilon = \frac{1}{2} \left(1 + \frac{9}{2\beta a}\right)$$

303

304 The expression in equation (5c) (Urick, 1948) accounts for viscous losses for $x \ll 1$; $\delta = \rho_s/\rho_w$
 305 and $\beta = \sqrt{\omega/2\nu}$, where $\omega = 2\pi f$ is the acoustic angular frequency, ν the kinematic viscosity for
 306 water, ρ_w is the density of water and ρ_s is the density of the solid particles. The normalised
 307 total cross-section is given by the addition of the scattering and viscous terms, $\chi_{iv} = \chi_i + \chi_v$.

308

309 To represent the ensemble scattering by a suspension with a range of particle sizes, the
 310 intrinsic scattering values are integrated over the particle number size probability density
 311 function, $P_j^n(a)$, where $j=b$ (bed) or s (suspension), to yield f and χ , the ensemble scattering
 312 characteristics:

313

$$f(x_o, z) = \left[\frac{\int_0^\infty a P_j^n(a, z) da \int_0^\infty a^2 f_i(x, z)^2 P_j^n(a, z) da}{\int_0^\infty a^3 P_j^n(a, z) da} \right]^{1/2} \quad (6a)$$

314

$$\chi(x_o, z) = \frac{\int_0^\infty a P_j^n(a, z) da \int_0^\infty a^2 \chi_{iv}(x, z) P_j^n(a, z) da}{\int_0^\infty a^3 P_j^n(a, z) da} \quad (6b)$$

315

$$a_o(z) = \int_0^\infty a P_j^n(a, z) da \quad (6c)$$

316

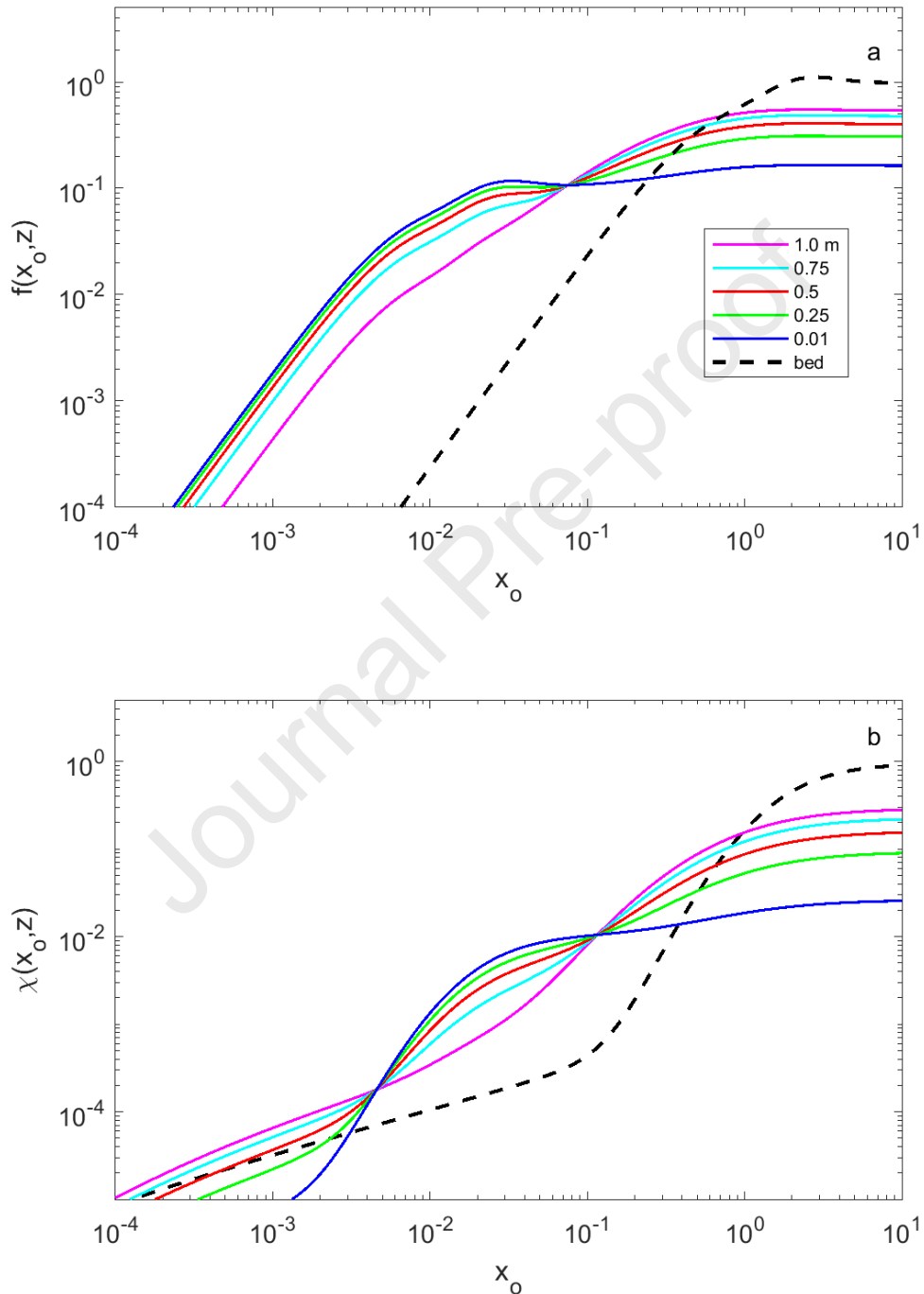
317 To obtain the scattering characteristics of the bed and suspended sediments, equation (6) was
 318 evaluated using equation (5) with equations (2) and (4). For the calculations $\rho_s=2600 \text{ kgm}^{-3}$,
 319 $\rho_w =1027 \text{ kgm}^{-3}$, and $\nu=1.10^{-6} \text{ m}^2\text{s}^{-1}$. The ensemble average form function, $f(x_o, z)$, and
 320 normalised total scattering and viscous cross-section, $\chi(x_o, z)$, are plot against $x_o=2\pi a_o f/c$
 321 respectively in figures 5a and 5b.

322

323 The commonly employed non-dimensional plots in figure 5 indicate different scattering
 324 characteristics for the suspended sediments and the bed. In figure 5a, $f(x_o, z)$ has higher values
 325 for the suspension than the bed for $x_o \leq 0.1$, and smaller values for $x_o \geq 1$. These dissimilarities
 326 are associated with the different forms for $P_b^n(a)$ and $P_s^n(a, z)$, and due to the value of a_o for
 327 the bed being approximately two orders of magnitude greater than that for the suspension.
 328 Also, for the suspension below $x_o \approx 0.1$, the trend is for $f(x_o, z)$ values to decrease with height
 329 above the bed, while above this value for x_o , the reverse is the case. This crossover in
 330 suspension scattering characteristics is considered to be associated with Rayleigh scattering
 331 when $x_o \ll 1$ and a convergence towards geometric scattering for larger values of x_o . Figure
 332 5b shows comparable differences to those identified in figure 5a, with similar variations in
 333 $\chi(x_o, z)$ between the suspension and the bed and within the suspension itself for the reasons
 334 given above. There is also the additional factor of viscous absorption, which introduces an
 335 increase in $\chi(x_o, z)$ with height above the bed below $x_o \approx 0.005$. Plotting the scattering
 336 characteristics in the customary non-dimensional form shown in figure 5 indicates

337 significantly different scattering characteristics between the suspended sediments and the
 338 bed, which could be considered to have important implications for acoustic inversions.

339



340

341 Fig 5. a). Selected form function, $f(x_o, z)$ and b) total normalised cross-section, $\chi(x_o, z)$ with x_o ,
 342 for suspended sediments between 0.01-1.0 m above the bed and for the bed sediments (—
 343 —). The legend provides the values of z for the individual suspension curves.

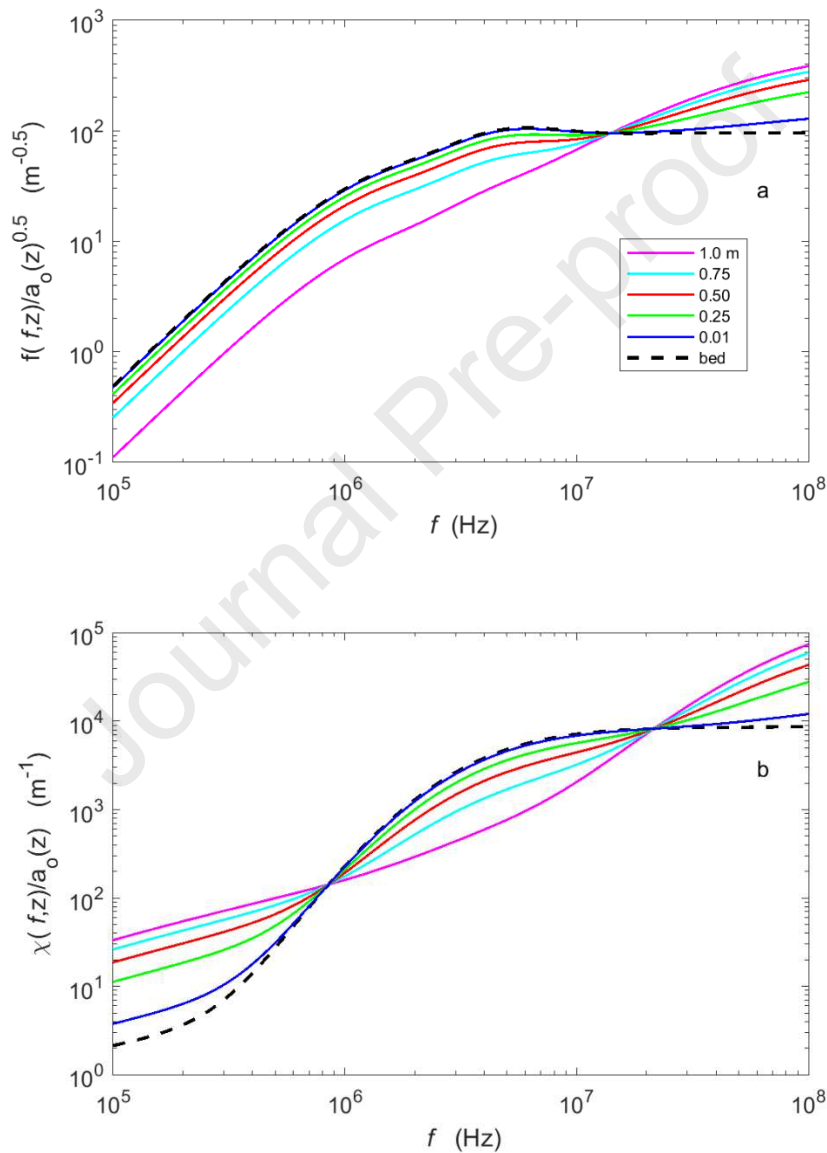
344

345 However, inspection of equation (9) shows $f(f, a_o(r))$ and $\chi(f, a_o(r))$ are divided respectively by346 $\sqrt{a_o(r)}$ and $a_o(r)$, where $r=r_b-z$ is the range from the transceiver and r_b is the range to the bed.

347 Therefore a more representative description of the scattering characteristics for the present

348 study would be $f(f, z)/\sqrt{a_o(z)}$ and $\chi(f, z)/a_o(z)$ with frequency f .

349



350

351

352 Fig 6. Selected modified scattering characteristics for; a) $f(f, z)/\sqrt{a_o(z)}$ and b) $\chi(f, z)/a_o(z)$,353 with frequency, f , for suspended sediments between 0.01-1.0 m above the bed and for the bed354 sediments (— —). The legend provides the values of z for the individual suspension curves.

355

356 Using these forms in figure 6 allows for a readier comparison between values for the bed and
357 the suspension. The bed and suspension characteristics now coalesce and follow the same
358 trends in the Rayleigh, geometric and viscous regimes as considered above.

359

Journal Pre-proof

360

4. Particle size and concentration profile

361 Formulations for the profiles of mean particle size and concentration were required to
 362 examine the scattering from mixed sediment suspensions. The mean particle size profiles, for
 363 mass, $a_c(z)$, and number, $a_n(z)$ are prescribed by the form of the suspension given in equation
 364 (4b) and are expressed as:

365

$$a_c(z) = \int_0^{\infty} aP_s^c(a, z) da \quad (7a)$$

366

$$a_n(z) = \int_0^{\infty} aP_s^n(a, z) da \quad (7b)$$

367

368 The forms for the profiles using equation (7) are presented in figure 7a. The figure shows a
 369 steady reduction in $a_c(z)$ with height above the bed as the sand content in suspension reduces,
 370 while the profile for $a_n(z)$ is very different to that of $a_c(z)$, with $a_n(z)$ being significantly
 371 smaller and almost uniform with height above the bed.

372

373 Two commonly used concentration profiles profile were adopted for the analysis. These were
 374 based on a Rouse power law (Rouse, 1937; Soulsby, 1997) and an exponential formulation
 375 (Schmidt, 1925; Nielsen, 1992). The power law was given by:

376

$$C(z) = C_o \left(\frac{z}{z_o} \right)^{-\gamma} \quad (8a)$$

377

378 C_o is the reference concentration at $z_o=0.01$ m and $\gamma=w_s/\kappa u_*$ is the Rouse parameter where w_s
 379 is the sediment fall velocity, κ is the von Karman constant and u_* is the form drag frictional
 380 velocity, a typical value of $\gamma=1.0$ was adopted for the modelling (Cheng et al., 2013). The
 381 exponential expression used was:

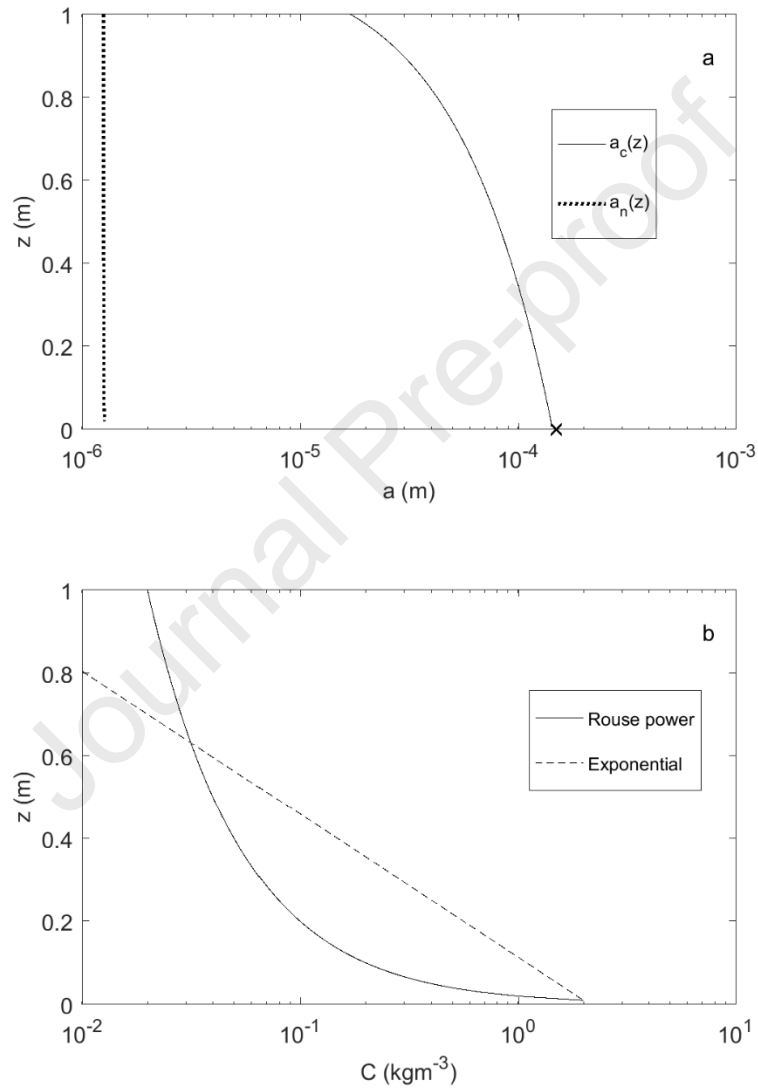
382

$$C(z) = C_o e^{-(z-z_o)/L_s} \quad (8b)$$

383

384 L_s is a vertical mixing length dependent on bed roughness and for the present study was set to385 0.15 m (van der Werf et al., 2006). $C_o = 2.0 \text{ kgm}^{-3}$ in both cases (Rose and Thorne, 2001).

386



387

388

389 Fig 7 Profiles of; a) mean suspended particle radius, for mass $a_c(z)$ (—) and number $a_n(z)$ (•••)390 and b) mass concentrations, $C(z)$, with height, z , above the bed, for the Rouse power (—) and391 exponential (---) forms. The mean bed mass radius, $a_{cb}(x)$, is shown in a).

392

393 The form for the two expressions is presented in figure 7b and show the expected steady
394 reduction in concentration with height above the bed. It is the scattering characteristics shown
395 in figure 6, coupled with the profiles given in figure 7, which are used in the present analysis
396 to compute the backscatter signals to be used in the inversions to obtain acoustic profiles of
397 suspended sediment mean mass particle size, $a_m(z)$ and concentration $M(z)$.

398

399

Journal Pre-proof

400 **5. Backscattered signal and acoustic inversions.**

401

402 *5.1 Calculation of the backscattered signal from the mud-sand suspension.*

403 Acoustic scattering theory for suspensions of sediments in a fluid is well developed (Thorne
404 and Hurther, 2014 and references therein). Under conditions of incoherent scattering the
405 mean square backscattered signal, $V_m^2(r)$, from a suspension with mass concentration, $C(r)$,
406 insonified with a piston transceiver, can be expressed as:

407

$$V_m^2(r) = \left(\frac{K(r) \mathfrak{R}}{r\psi(r)} \right)^2 C(r) e^{-4(r\alpha_w + \alpha_s(r))} \quad (9)$$

408

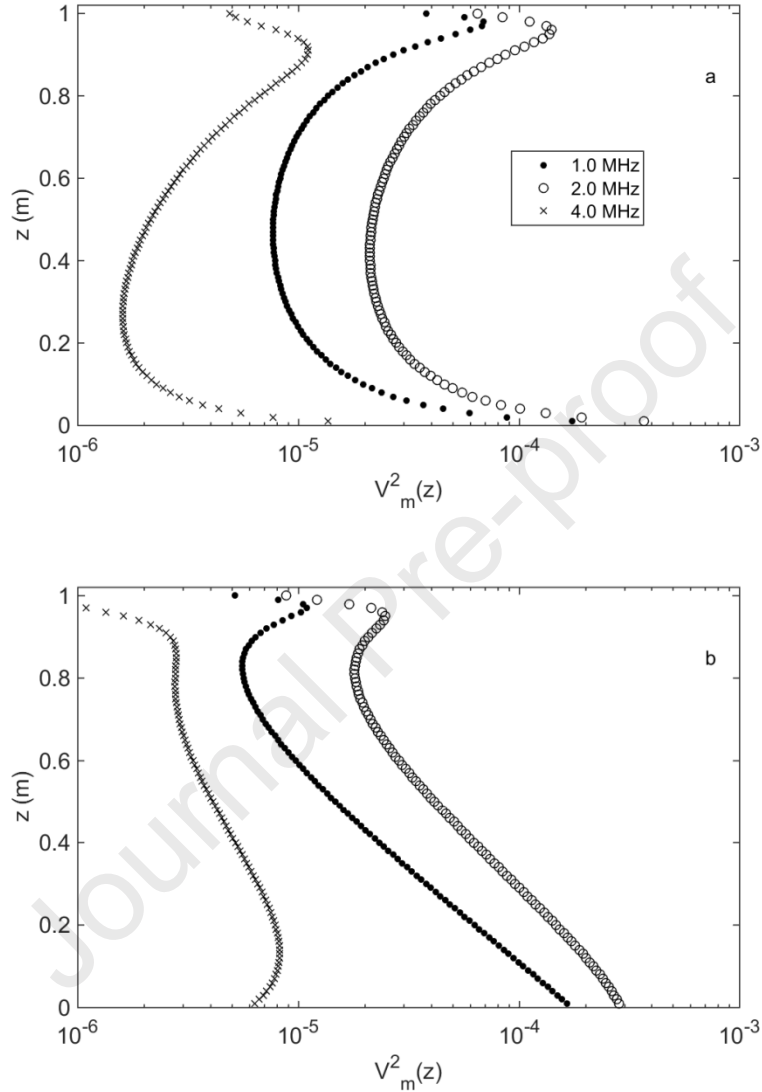
$$K(r) = \frac{f(f, a_o(r))}{(\rho_s a_o(r))^{1/2}}, \quad \alpha_s(r) = \int_0^r \xi(r) C(r) dr, \quad \xi(r) = \frac{3\chi(f, a_o(r))}{4\rho_s a_o(r)}$$

409

410 In the above, r is the range from the transceiver, $\psi(r)$ accounts for the departure from
411 spherical spreading within the transceiver nearfield (Downing et al., 1995), \mathfrak{R} is a system
412 constant (Betteridge, et al., 2008) and α_w is attenuation due to water absorption. Equation (9)
413 can be readily evaluated; equation (6) provides $f(f, a_o(r))$, $\chi(f, a_o(r))$ and $a_o(r)$, equation (8)
414 provides $C(r)$, $\psi(r)$ was calculated for the transceivers using nominal diameters of 0.01 m and
415 \mathfrak{R} values were obtained from a manufacturer's calibrations for an ABS. For the present study,
416 the transceivers were mounted at 1.0 m above the bed with a vertical sampling resolution of
417 0.01 m and having 100 range bins. The computed backscattered signals from the two
418 modelled concentration profiles at frequencies of 1.0, 2.0 and 4.0 MHz are shown in figure 8.
419 The backscattered signal from the Rouse power law concentration is given in figure 8a, this
420 shows mean square signal profiles with a peak in the signal at approximately the boundary
421 between the near field and far field, within $r=0.1$ m of the transceivers, at a height between
422 $z=0.9-1.0$ m. Above the peak the signal reduces due to the form of $\psi(r)$ and below the peak,
423 even though the particle size and concentration are increasing, the backscattered signal
424 reduces due to the spherical spreading and attenuation of the two way propagation. Below

425 about $z \approx 0.2$ m the higher concentrations begin to dominate the backscattered signals, which
 426 increases as the bed is approached.

427



428

429

430 Fig 8 Profiles of the mean square backscattered signal, $V_m^2(z)$ with height, z , above the bed
 431 for three frequencies propagating through; a) the Rouse power law and b) the exponential,
 432 concentration profiles.

433

434 Figure 8b shows that the backscatter from the exponential concentration profile has a similar
 435 reduction in signal level in the near field, while in the far field the forms are somewhat
 436 different. Below $z \approx 0.8$ m the interplay between, spherical spreading, attenuation, particle size

437 and concentration leads to backscatter signals at 1.0 MHz and 2.0 MHz showing an increase
 438 with reducing z , while at 4.0 MHz there is a slowly varying backscatter signal between $z=0.1$ -
 439 0.9 m, with a reduction below $z=0.1$ m as the bed is approached and sediment attenuation
 440 begins to dominate the 4.0 MHz backscattered signal.

441

442 *5.2 Inversion of the backscattered signals.*

443 To acoustically obtain profiles of the suspended concentration and mean number particle
 444 radius, requires an iterative solution to an implicit equation computed over a range of radii.
 445 Rearranging equation (9) gives:

446

$$M(r) = \left(\frac{r\psi(r)}{K(r)\mathfrak{R}} \right)^2 V_m^2(r) e^{4(r\alpha_w + \alpha_s(r))} \quad (10)$$

447

$$\alpha_s(r) = \int_0^r \xi(r)M(r) dr$$

448

449 $M(r)$ is used to represent the acoustic estimate of the suspended concentration $C(r)$. Equation
 450 (10) is implicit because $M(r)$ is on both sides of the equation due to $\alpha_s(r)$. To obtain an initial
 451 estimate for M , the sediment attenuation is initially neglected to give M_o

452

$$M_o(r) = \left(\frac{r\psi(r)}{K(r)\mathfrak{R}} \right)^2 V_m^2(r) e^{4r\alpha_w} \quad (11)$$

453

454 An improved estimate for M can be obtained using,

455

$$M_1(r) = M_o(r) e^{4\alpha_{so}} \quad (12)$$

456

457 Where α_{so} is calculated using M_o . Generally, equation (12) can be written as,

458

$$M_{k+1}(r) = M_o(r)e^{4\alpha_{sk}} \quad (13)$$

459

460 Equation (13) is iterated until a convergence criterion has been satisfied and the value for
 461 $M(r)$ estimated. Equations (11)-(13) were computed over a range of particle radii which
 462 covers the expected mean particle sizes in suspension. For the present study the range was
 463 $a_o=0.05 \mu\text{m}$ to $250 \mu\text{m}$ in steps of $0.05 \mu\text{m}$. This covered the range from clay through to
 464 coarse sand. To obtain an acoustic estimate of mean number particle size, the mean and
 465 standard deviation of $M(r)$ were calculated as:

466

$$\bar{M}(a, r) = \frac{1}{N} \sum_{j=1}^N M_j(a, r) \quad \sigma_M^2(a, r) = \frac{1}{N-1} \sum_{j=1}^N (M_j^2(a, r) - \bar{M}(a, r)^2) \quad (14)$$

467

468 Where N is the number of acoustic frequencies, in the present case $N=3$. The ratio below is
 469 now formed,

470

$$\phi(a, r) = \left(\frac{\sigma_M(a, r)}{\bar{M}(a, r)} \right) \quad (15)$$

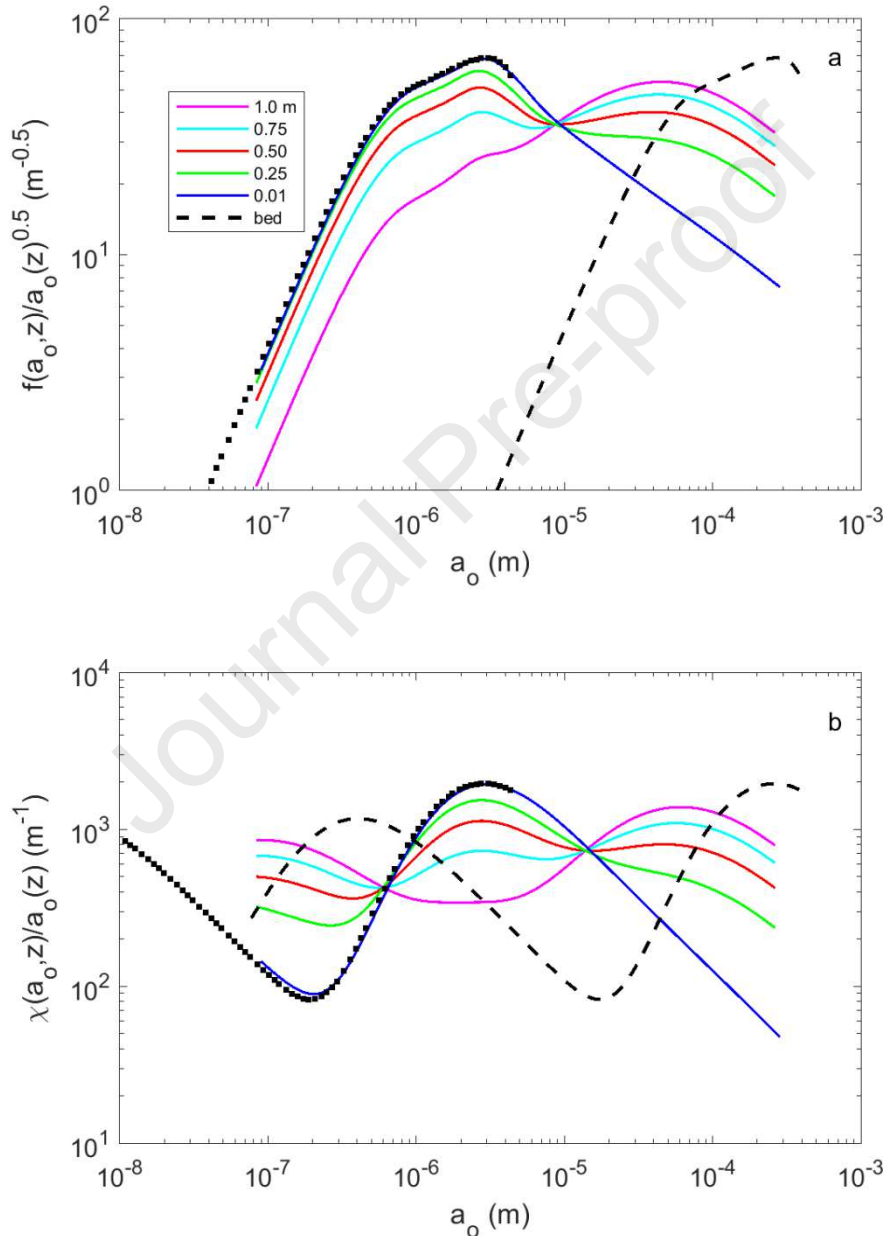
471

472 The minimum value of $\phi(a, r)$ is used to specify the acoustic values of mean number size,
 473 $a_n(r)$, and the mass concentration, $M(r)$, at range r . This methodology identifies the particle
 474 size at which the concentrations for the different frequencies converge and have minimum
 475 normalized variance. This provides values for $a_n(r)$ and $M(r)$ in the first range bin from the
 476 transceiver at $r=0.01 \text{ m}$. The computation is repeated for each range bin downwards towards
 477 the bed, with the accumulating sediment attenuation accounted for, to provide profiles of
 478 $a_n(z)$ and $M(z)$. Further details on the inversion methodology are given in Thorne and Hurther
 479 (2014).

480

481 To evaluate equation (10) over a range of mean mass radii the scattering characteristics
 482 presented in figure 6 were not used, because unlike the attenuation scattering component, the
 483 viscous attenuation varies differently with x_o as frequency or particle size is varied.

484 Therefore, the scattering characteristics were calculated for each of the three frequencies
 485 using the size distributions derived from equation (4b) as $a_o(z)$ was varied and $\sigma(z)/a_o(z)$
 486 remained constant at 0.3 and 1.0 for the sand and mud components respectively. Equation (6)
 487 was again used to evaluate $f(a_o, z)$ and $\chi(a_o, z)$ and for consistency with figure 6,
 488 $f(a_o, z)/\sqrt{a_o(z)}$ and $\chi(a_o, z)/a_o(z)$ are plotted in figure 9 at the same selected heights above the
 489 bed as in figure 6.



490

491

492 Fig 9. The 2.0 MHz modified scattering characteristics with mean particle radius, a_o , for the
 493 suspended sediments between 0.01-1.0 m above the bed and the bed sediments (— —) for; a)

494 $f(a_o, z)/\sqrt{a_o(z)}$ and b) $\chi(a_o, z)/a_o(z)$. The dotted curve (•) is the bed scattering characteristics
 495 translated along the a_o axis. The legend provides the values of z for the individual curves.

496

497 The calculations shown in figure 9 are for 2.0 MHz, with similar curves being calculated for
 498 1.0 MHz and 4.0 MHz. For the inversion lookup tables, a_o , $f(a_o, z)$ and $\chi(a_o, z)$ were generated
 499 at each of the three frequencies for each 0.01m height above the bed over the broad range of
 500 mean number radii shown in figure 9. As with figure 5, the suspension and bed scattering
 501 characteristics are separated due to the approximate two orders of magnitude difference in a_o .
 502 If the bed scattering characteristics are translated along the a_o axis by this difference, as
 503 indicated by the dotted curves in figure 9, the scattering characteristics coalesce as in figure
 504 6. The variations in the scattering characteristics with a_o follow the same trends as considered
 505 above for figures 5 and 6 and are associated with Rayleigh scattering below the cross-over
 506 point, $a_o \approx 10 \mu\text{m}$ with convergence to geometric scattering for larger a_o . For the 1.0 MHz and
 507 4.0 MHz scattering characteristics the cross-over points occur $a_o \approx 20 \mu\text{m}$ and $a_o \approx 5 \mu\text{m}$
 508 respectively. The main difference between figure 9 and figures 5 and 6 is in figure 9 the
 509 dependency is upon the variable $a_o(z)$ with a fixed frequency, which due to $\sqrt{a_o}$ and a_o in the
 510 denominator of $f(a_o, z)/\sqrt{a_o(z)}$ and $\chi(a_o, z)/a_o(z)$ leads to scattering characteristics which plot
 511 somewhat differently to figures 5 and 6, where $a_o(z)$ is fixed and frequency is varied.

512

513 *5.3 Inversion when the form of $P_s^c(a, z)$ is known*

514 In the first instance, it was assumed a priori knowledge was available for $P_s^c(a, z)$ in the form
 515 given in equation (4b) and converted to $P_s^n(a, z)$ using equation (2). Carrying out an inversion
 516 as outlined above, equations (10)-(15) were solved over the range of a_o between 0.2-300 μm
 517 in step intervals of 0.02 μm , using the suspension scattering characteristics shown in figure 9
 518 to yield acoustical mean number particle radius, $a_n(z)$ and suspended concentration, $M(z)$.
 519 The values for $a_n(z)$ obtained from the inversion were converted to $a_m(z)$, the acoustic
 520 estimate of mean particle mass size, using equation (16) below:

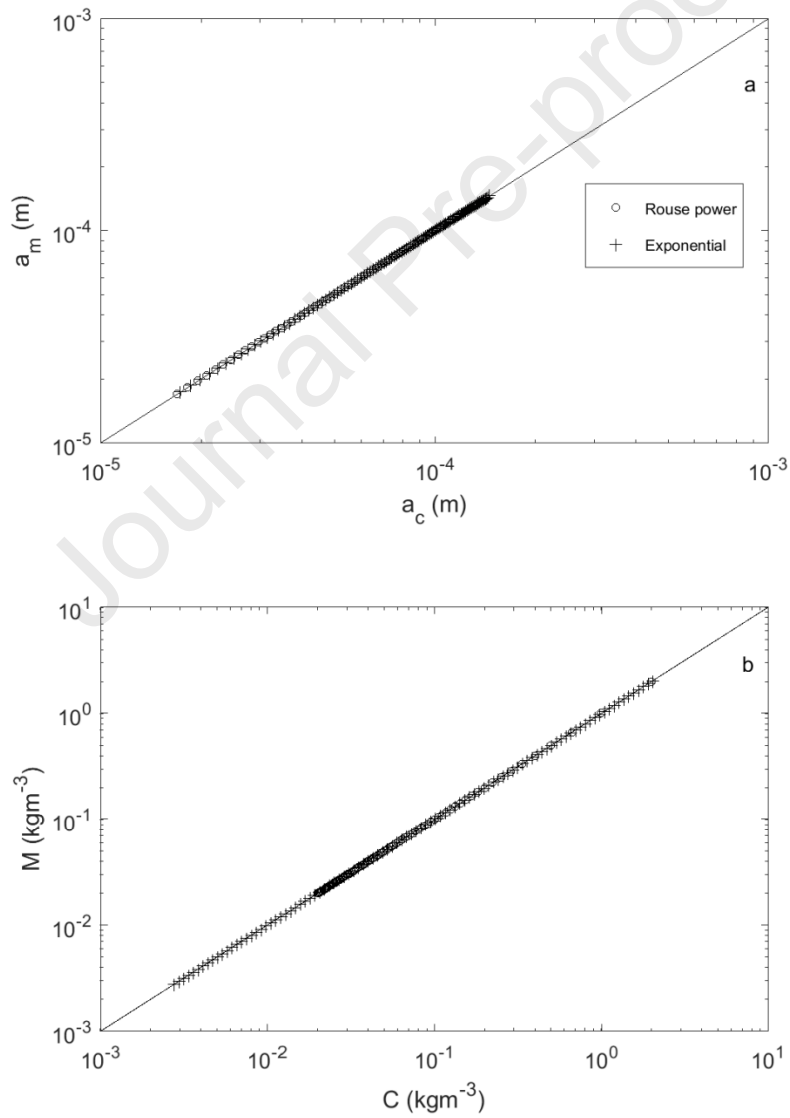
521

$$a_m(z) = a_n(z) \left[\frac{\int_{a_1}^{a_2} a P_s^c(a, z) da}{\int_{a_1}^{a_2} a P_s^n(a, z) da} \right] \quad (16)$$

522

523 Acoustic values for $a_m(z)$ and $M(z)$ were compared with the input profiles $C(z)$ and $a_c(z)$,
 524 used to calculate the backscattered signals given in figure 8. The results of the comparison are
 525 shown as regression plots in figure 10.

526



527

528

529 Fig 10. Regression plots of the inverted acoustic output profiles with the input profiles for; a)
 530 mean mass size, $a_m(z)$ and $a_c(z)$ and b) concentration, $M(z)$ and $C(z)$.

531

532 It can be clearly seen that the output from the inversion compares well with the input profiles
 533 for both the mean mass particle radius and concentration. Linear regression analysis gives
 534 regression coefficients, gradients and intercepts for the Rouse power and exponential mass
 535 profile respectively of 1.0000, 1.0015, 0.0000 and 1.0000, 1.0015, 0.0000 for the size and
 536 1.0000, 1.0014, -0.0001 and 1.0000, 0.9988, 0.0004 for the concentration. The slight
 537 departures from unity and zero for the gradients and intercept respectively are associated with
 538 the discretisation of both the lookup tables and a_o for the calculations. It is sometimes
 539 indicated (e.g. Brand et al., 2020) that in a mixed suspension environment, acoustic
 540 backscattering would be insensitive to the clay component, however, this is belied by the
 541 results in figure 10, which show that the fine components of the suspension are captured in
 542 the inversion. Therefore the analysis in this section was not only conducted as an assessment
 543 of the veracity of inversion methodology, but also to highlight that with the correct ensemble
 544 scattering characteristics in a mixed mud and sand environment, the suspension particle size
 545 and concentration profiles can be accurately reconstructed. This will be seen to not be the
 546 case for the scenarios below.

547

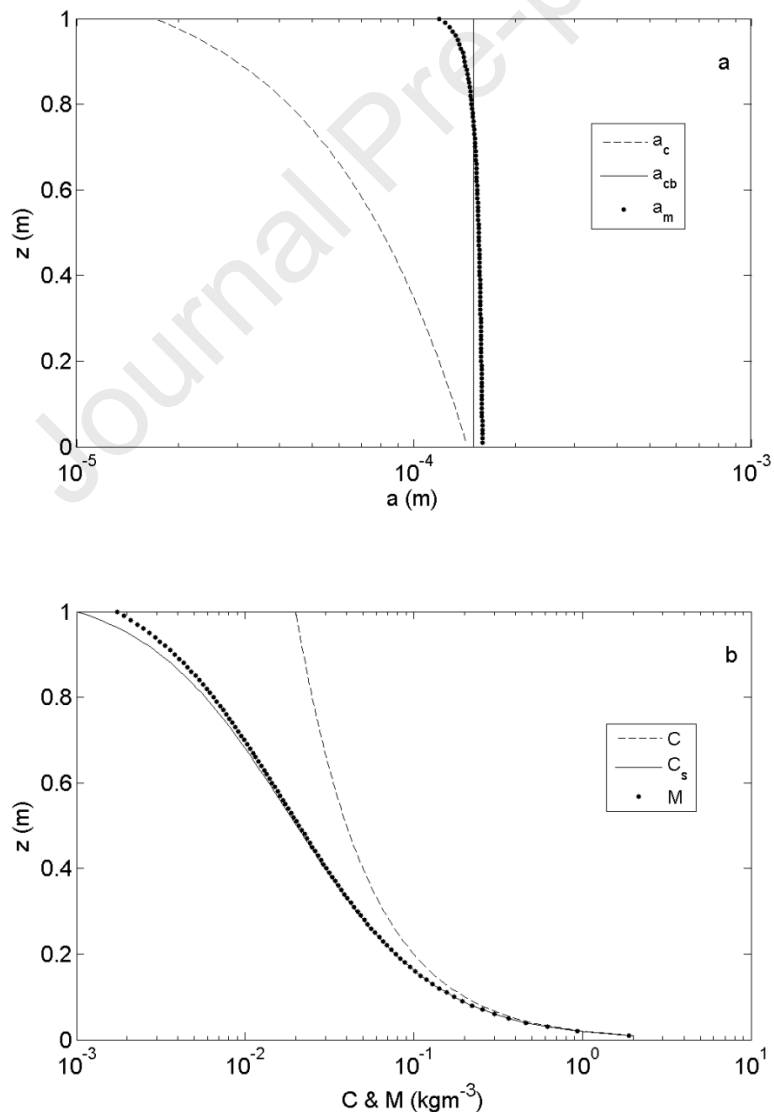
548 *5.4 Inversion when the form of $P_b^c(a)$ is known for the sand component*

549 The results presented in figure 10 are for the case when the form of the mass size distribution,
 550 $P_s^c(a,z)$, is a priori known above the bed, but the profiles for $a_c(z)$ and for $C(z)$ are unknown
 551 and these were obtained from the acoustic inversion which yields $a_m(z)$ and $M(z)$. Invariably
 552 in field studies such details of $P_s^c(a,z)$ over time are not available and consequently bed
 553 sediments collected from the study site are used to carry out the acoustic inversion (Vincent
 554 and Green, 1990; Hanes, 1991; Vincent et al., 1991; Hay and Sheng, 1992; Thorne et al.,
 555 1993; Sheng and Hay, 1995; Osborne and Vincent, 1996; Thorne and Hardcastle, 1997;
 556 Green and Black 1999; Lee et al., 2004; Bolanos et al., 2012; Moate et al., 2016). It is this use
 557 of bed sediments for the inversion over broadly mixed sediments that is investigated here.

558

559 To carry out the acoustic inversions for suspended mean mass size and concentration using
 560 the bed sediments, the same approach as used in section 5.3 was adopted, with equations
 561 (10)-(15) solved over a range of a_0 using the scattering characteristics of the bed shown in
 562 figure 9. This resulted in the mean mass particle radii and suspended concentrations profiles
 563 shown in figures 11 and 12. In the figures dashed and solid lines are shown. The dashed line
 564 in the figures are profiles from equations (7) and (8) and are the same as those shown in
 565 figure 7 for $a_c(z)$ and $C(z)$. The solid lines are solely the sandy component of the suspended
 566 sediment, with equation (7) evaluated using $P_b^c(a)$, which results in a uniform mean mass
 567 particle size of $a_{cb}=150 \mu\text{m}$ with height above the bed and concentration profiles given by a
 568 modification of equation (8), represented by $C_s(z)=\theta(z)C(z)$. The results from the acoustic
 569 inversions are given by the solid circles.

570



571

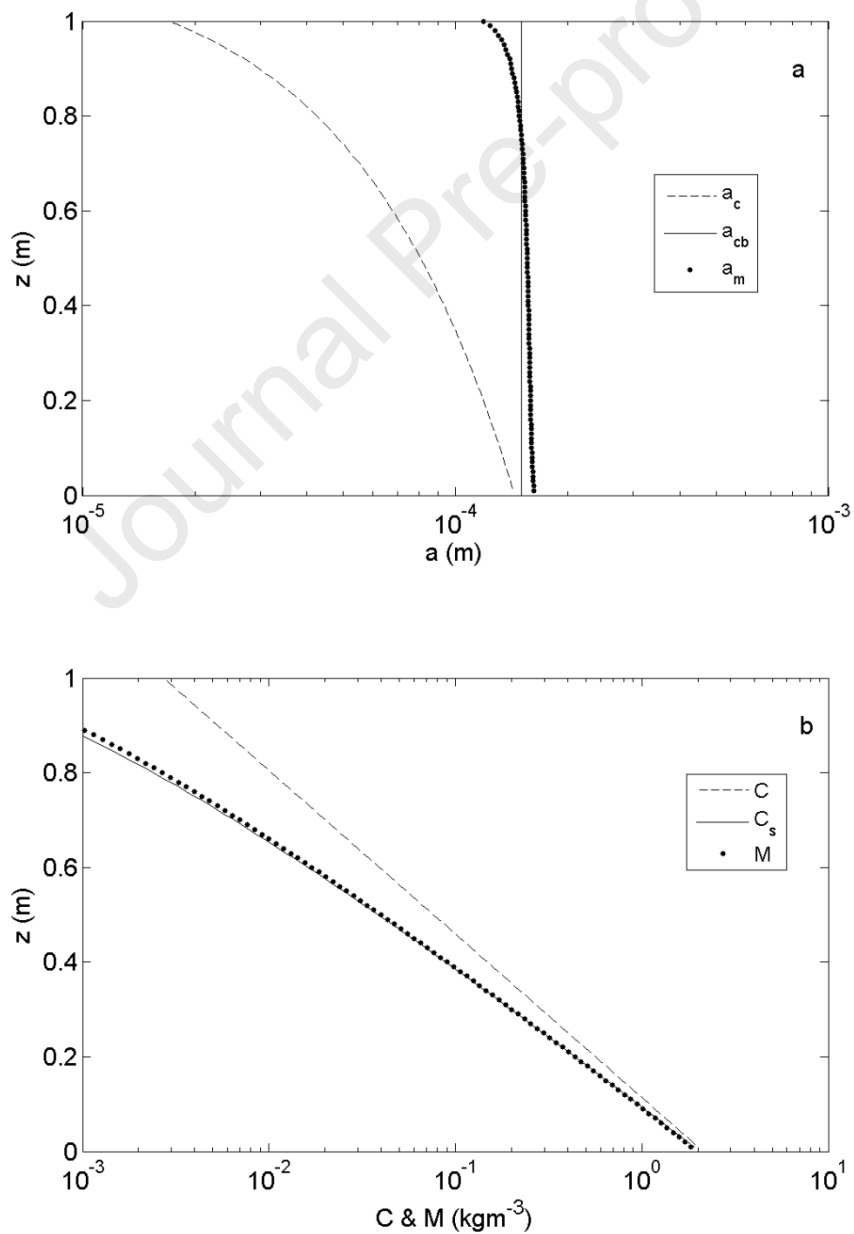
572

573 Fig 11. Inversion using $P_b^n(a)$ with 0% mud. a). Comparisons for the Rouse power profile of
 574 a) mean mass radius for the mixed suspended sediments, $a_c(z)$ (---), the sand component of
 575 the bed sediments, a_{cb} (—), and the acoustic inversion $a_m(z)$ (•). b) The concentration for the
 576 mixed suspended sediments, $C(z)$ (---), the sand component of the suspended sediments,
 577 $C_s(z)$ (—), and the acoustic inversion $M(z)$ (•).

578

579

580



581

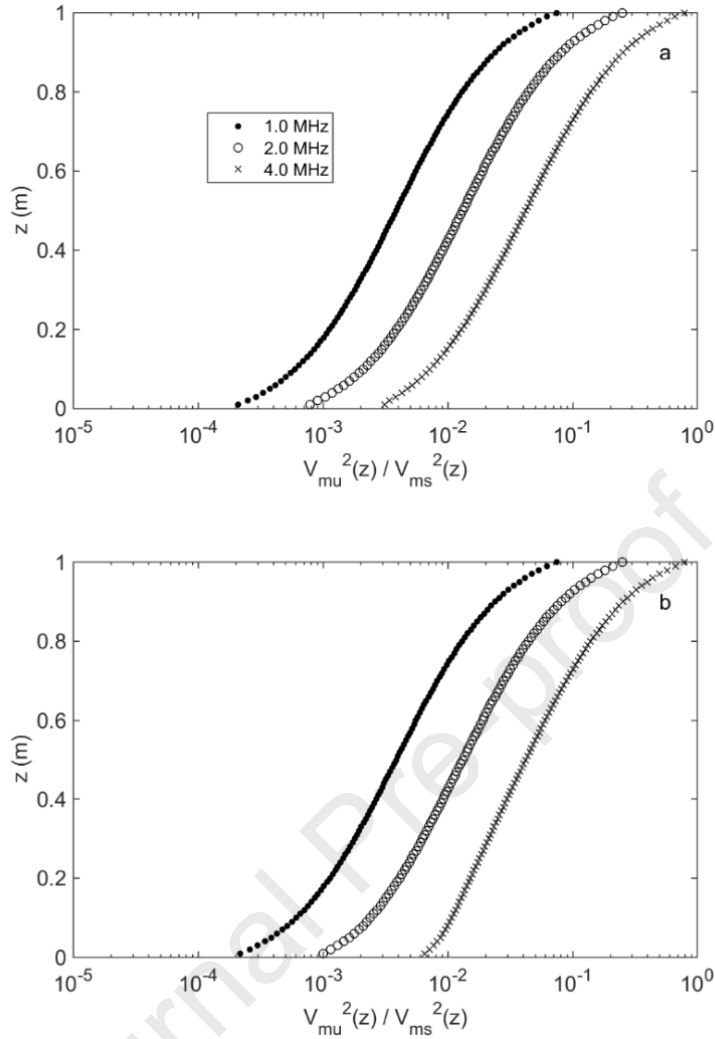
582

583 Fig 12. Inversion using $P_b^n(a)$ with 0% mud. Comparisons for the exponential profile of a)
584 mean mass radius for the mixed suspended sediments, $a_c(z)$ (—), the sand component of the
585 bed sediments, a_{cb} (—), and the acoustic inversion $a_m(z)$ (•). b) The concentration for the
586 mixed suspended sediments, $C(z)$ (—), the sand component of the suspended sediments,
587 $C_s(z)$ (—), and the acoustic inversion $M(z)$ (•).

588

589 It can be seen that using $P_b^c(a)$, that is a lognormal mass distribution with $\sigma(a,z)/a_c(z)=0.3$,
590 with equation (2), to obtain a lognormal $P_b^n(a)$ for the inversion, results in values for $a_m(z)$
591 and $M(z)$ which closely follow the uniform sand value of $a_{cb}=150 \mu\text{m}$ for the bed and the
592 sand component of the suspension, $\theta(z)C(z)$, for both the Rouse power and exponential
593 profiles. It is therefore the case, that when the dominant sand component of the bed sediments
594 is used for an inversion consisting of a mixture of sands and muds, with the muddy
595 component becoming increasingly dominant with height above the bed, the result is a profile
596 very comparable to the sandy component of the suspension.

597



598

599

600 Fig 13. Ratios of the components of the mean square backscatter signal in suspension from
 601 the mud, $V_{\text{mu}}^2(z)$, and the sand, $V_{\text{ms}}^2(z)$, for; a) Rouse power and b) exponential
 602 concentration profiles.

603

604 To examine the results presented in figures 11 and 12 the backscattered signal from the sandy
 605 and muddy components were computed separately. These were obtained by firstly calculating
 606 the suspension scattering characteristics using equation (6), with $P_s^n(a,z)$ derived from
 607 equation (2) using (4a) for the sandy component and with $\theta(z)=0$ in equation (4b) for the
 608 muddy component. Using the sand and mud scattering characteristics respectively with
 609 concentration profile components for sand, $C_s(z)=\theta(z)C(z)$, and mud, $C(z)-C_s(z)$, equation (9)
 610 was evaluated to provide the individual mean-square backscattering from the sand, $V_{\text{ms}}^2(z)$,
 611 and mud, $V_{\text{mu}}^2(z)$, components. The ratio of these two signals, $V_{\text{mu}}^2(z)/V_{\text{ms}}^2(z)$, with height

612 above the bed are shown for the power Rouse and exponential concentration profiles in figure
613 13. It can be clearly seen that the backscatter from the sand component dominates that from
614 the mud, even when the sandy component is only 5% of the total mass at $z=1.0$ m. It is the
615 combination of the dominance of the sand scattering component, coupled with the bed
616 lognormal particle number size distribution used to calculate the suspension ensemble
617 scattering characteristics, which leads to the inversions shown in figures 11 and 12.

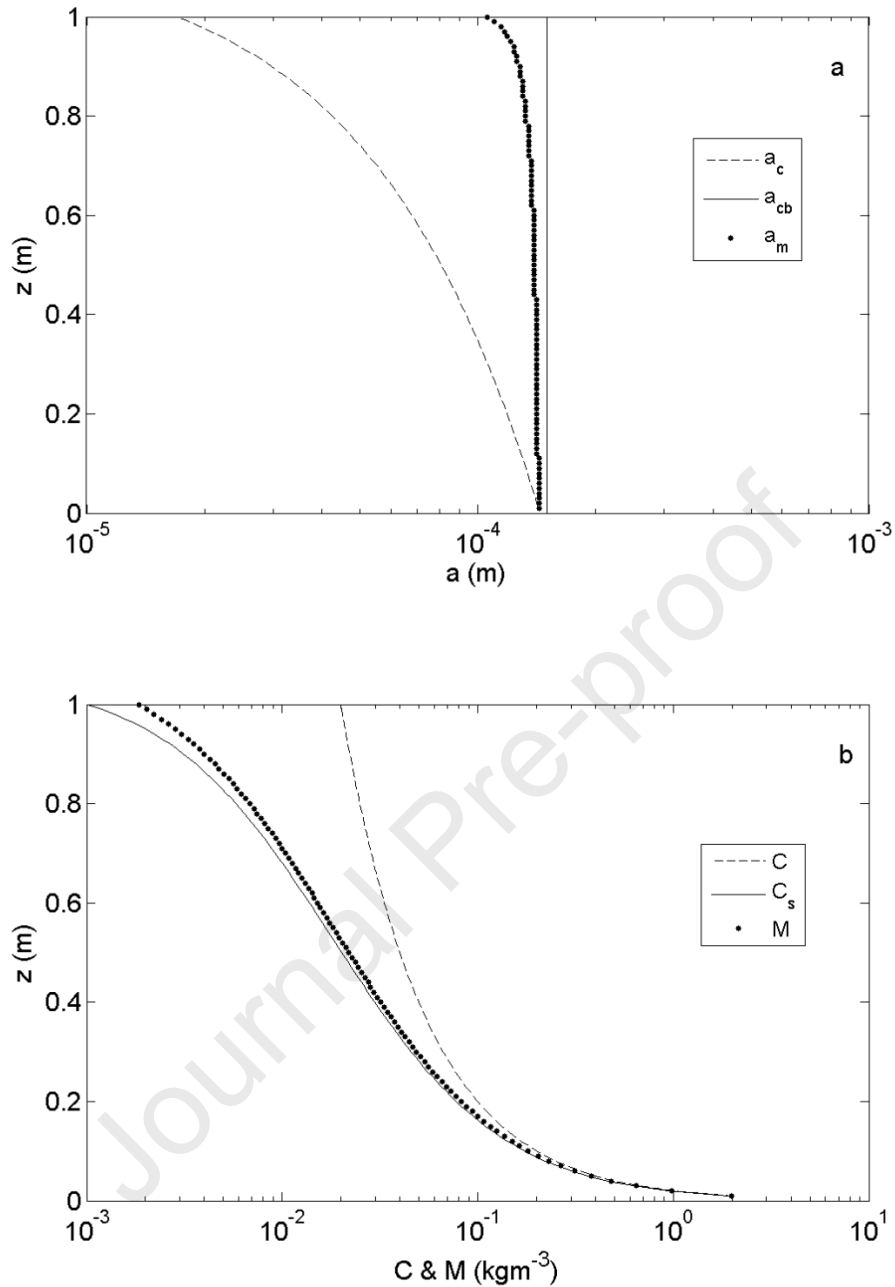
618

619 *5.5 Inversion when the form of $P_b^c(a)$ is known for the sand and mud component*

620 It was considered important to carry out an inversion with a size distribution not solely based
621 on the bed sand component, but one which also incorporated the mud component in the bed.
622 The interest being to assess if calculating the ensemble scattering characteristics using the
623 correct size distribution of the mud and sand components in the bed, resulted in an inversion
624 closer to the actual suspension, than that of solely using the sand component. To represent a
625 combined distribution for the bed, the suspension scattering characteristics closest to the bed,
626 shown in figure 9 at 0.01m above the bed, $P_s^n(a, 0.01)$, which had a 5% mud component, was
627 selected. The inversions for this scenario are shown in figures 14 and 15. The outcome is very
628 comparable to figures 11 and 12. This shows that even if the full-size distribution of the bed
629 is used to compute the scattering characteristics, the inversion still yields profiles for $M(z)$
630 and $a_m(z)$ which compare closely with the sandy components of the suspension. This outcome
631 is essentially due to the ensemble scattering characteristics used in the inversion being those
632 of a composition of 95% sand and 5% mud, which is not an accurate representation of the
633 suspension scattering characteristics, as opposed to the case in section 5.3.

634

635

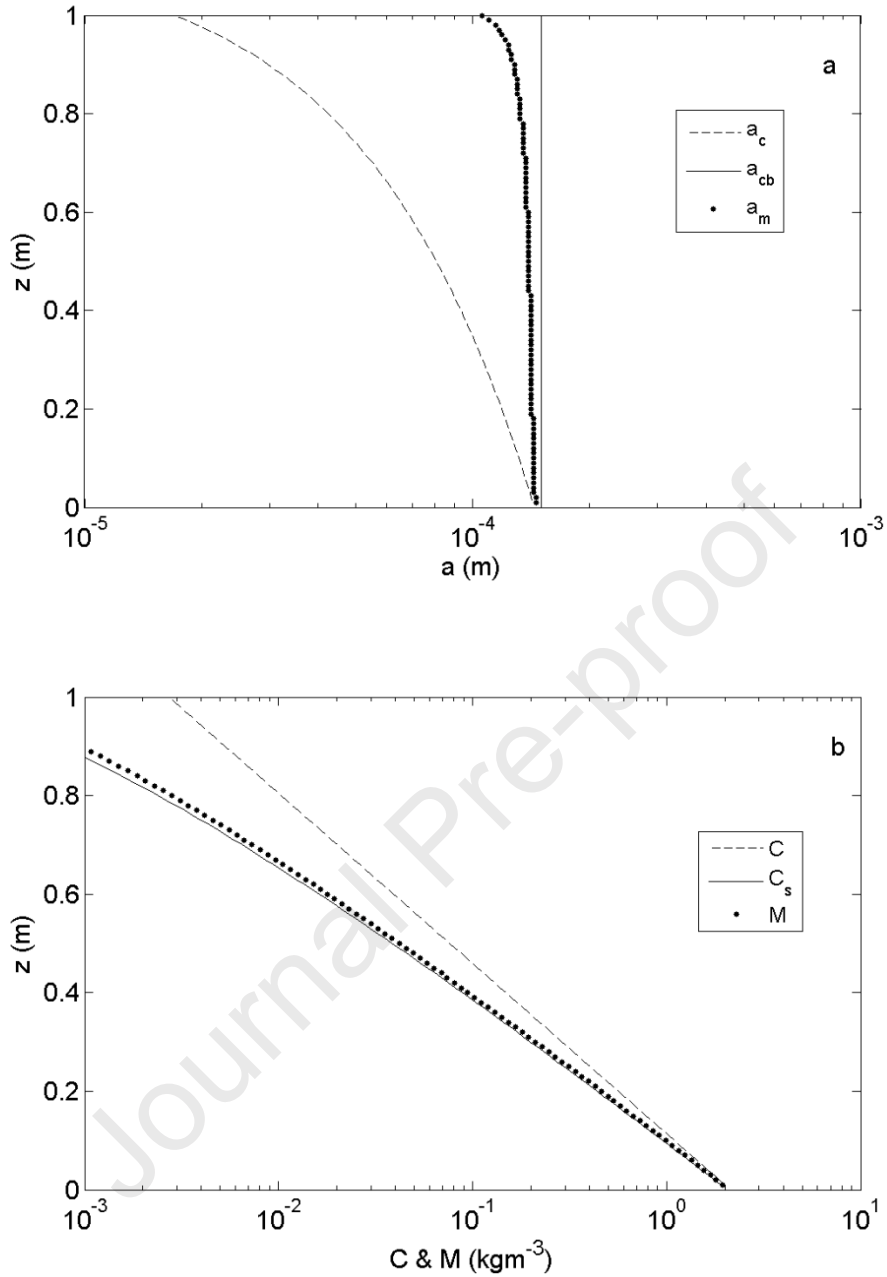


636

637

638 Fig 14. Inversion using $P_s^n(a, 0.01)$ with 5% mud. Comparisons for the Rouse power profile
 639 of a) mean mass radius for the mixed suspended sediments, $a_c(z)$ (---), the sand component
 640 of the bed sediments, a_{cb} (—), and the acoustic inversion $a_m(z)$ (•). b) The concentration for the
 641 mixed suspended sediments, $C(z)$ (---), the sand component of the suspended sediments,
 642 $C_s(z)$ (—), and the acoustic inversion $M(z)$ (•).

643



644

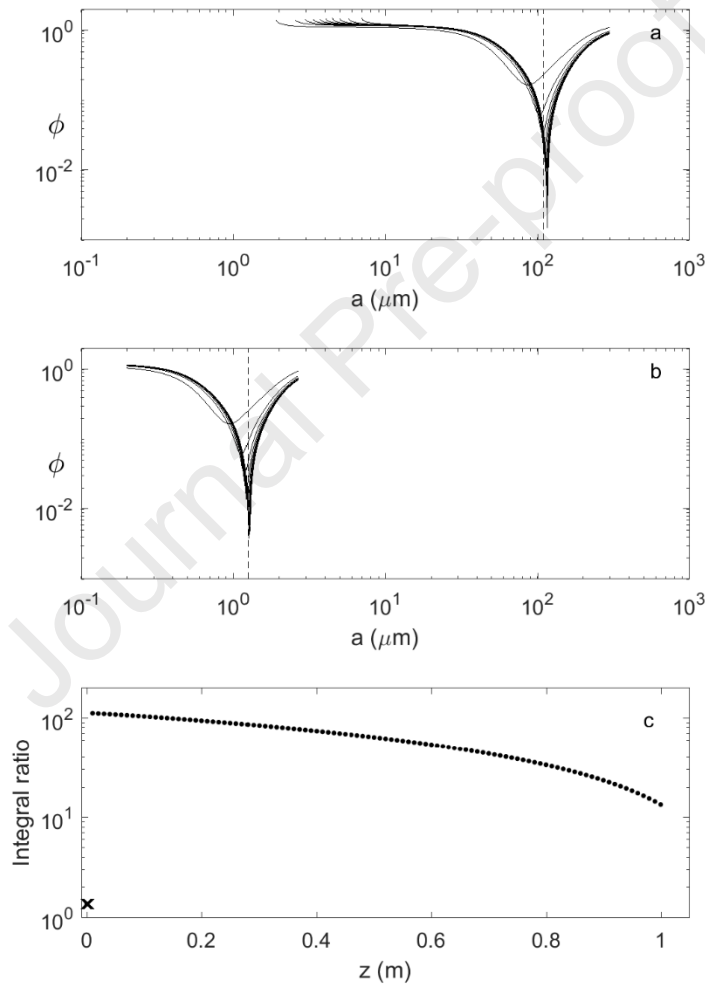
645

646 Fig 15. Inversion using $P_S^n(a, 0.01)$ with 5% mud. Comparisons for the exponential profile of
 647 a) mean mass radius for the mixed suspended sediments, $a_c(z)$ (---), the sand component of
 648 the bed sediments, a_{cb} (—), and the acoustic inversion $a_m(z)$ (•). b) The concentration for the
 649 mixed suspended sediments, $C(z)$ (---), the sand component of the suspended sediments,
 650 $C_s(z)$ (—), and the acoustic inversion $M(z)$ (•).

651

652 To shed some further insight on the results presented in figures 11, 12, 14 and 15 the
 653 variation of $\phi(a)$ with a is plotted in figures 16a and 16b. In figure 16a, when using $P_b^n(a)$ for
 654 the inversion, it can be seen that the minimum value for $\phi(a)$, which yields the profile for a_n ,
 655 occurs in the sandy regime between values of $a_n(z)=96-117 \mu\text{m}$ which are comparable with
 656 the mean number size for the bed of $a_{nb}=109 \mu\text{m}$. This is therefore consistent with using the
 657 bed lognormal particle size number distribution for the inversion, resulting in the plots shown
 658 in figures 11 and 12.

659



660

661

662 Fig 16. Plots of $\phi(a,z)$, equation (15), versus a for a) an inversion using $P_b^n(a)$ and b) an
 663 inversion using $P_s^n(a,0.01)$. c) The ratio of the integrals given in equation (16), bed (x),
 664 suspension (\bullet). The dashed lines are $a_{nb}=109 \mu\text{m}$ in a) and $a_n(z)=1.2 \mu\text{m}$ in b).

665

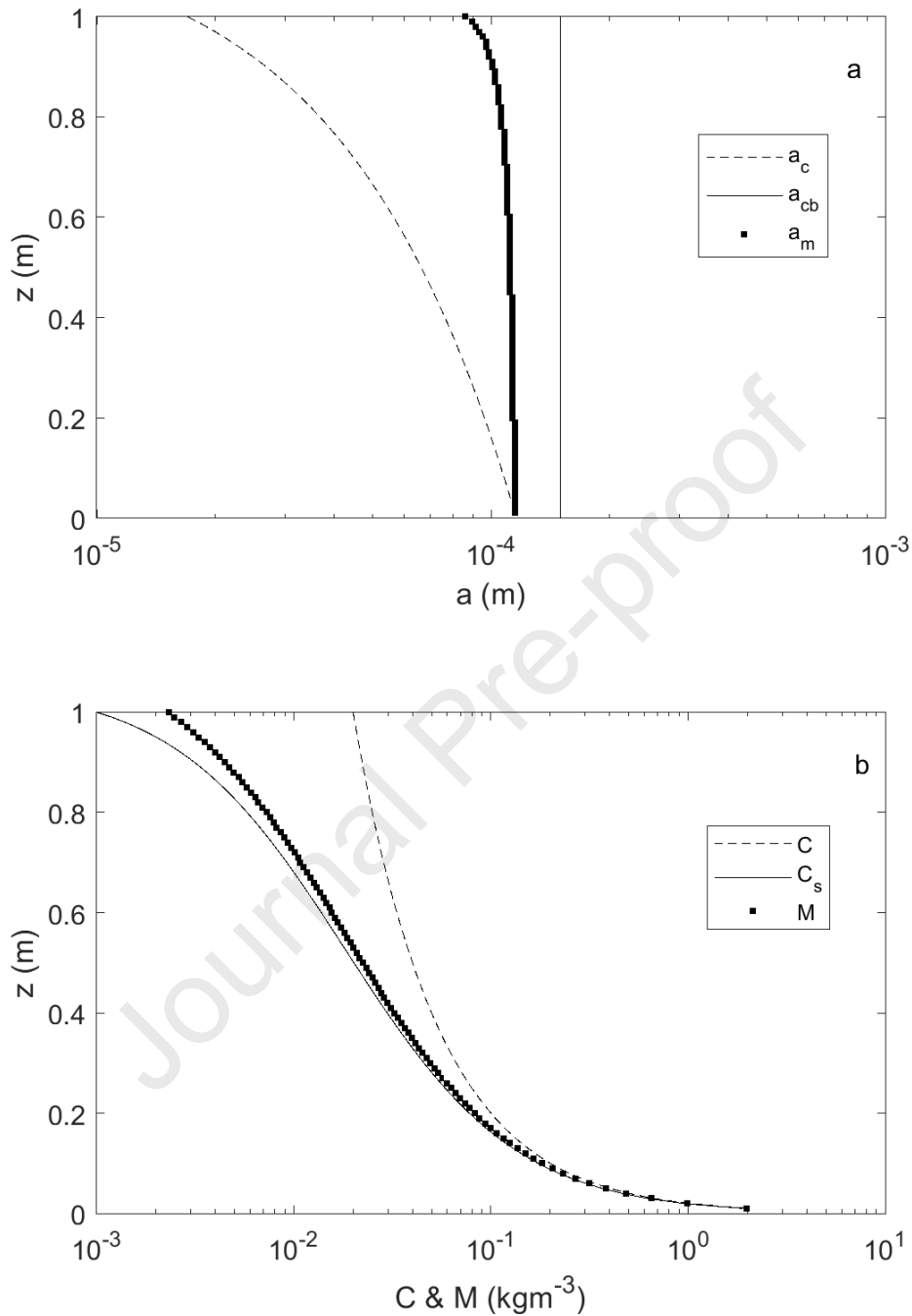
666 However, as shown in figure 16b, when the particle number size probability density
 667 distribution $P_s^n(a, 0.01)$ is applied in the inversion, with the 5% mud content, the minimum
 668 values for $\phi(a)$ occur in the mud regime, with a profile for mean number particle sizes
 669 $a_n(z)=0.94-1.28 \mu\text{m}$. These values are comparable with the suspension mean number particle
 670 size of $a_n(z)\approx 1.2 \mu\text{m}$ and not the sand size profile for a_m shown in figures 14 and 15. The
 671 explanation for this is revealed in figure 16c which shows the ratio of the integrals in
 672 equation (16) used to convert $a_n(z)$ to $a_m(z)$. For the lognormal bed particle size distribution,
 673 this ratio, shown by the cross, is close to unity having a value of 1.37, which yields values for
 674 $a_m(z)$ between 130-160 μm , which are close to the value for the bed mass mean size of
 675 $a_b=150 \mu\text{m}$. However, for the suspended sediments the integral ratio varies from 112 at 0.01
 676 m to 13 at 1.0 m above the bed. It therefore the integral ratio of 112 at 0.01 m above the bed,
 677 that translates the $a_n(z)=0.94-1.28 \mu\text{m}$ profile from the mud regime, to the sandy regime
 678 $a_m(z)=105-144 \mu\text{m}$ and leads to the results shown in figures 14 and 15.

679

680 *5.6 Inversion when the form of $P_b^c(a)$ is known for the sand with a large mud component*

681 The scenarios described above for sediments in an estuary of the type measured in the Dee,
 682 were for the case when the muddy fraction was a relatively small component of the total.
 683 However, riverine and estuarine environments are very variable and can be composed of a
 684 much higher mud fractions. Therefore to broaden the analysis and assess outcomes, the case
 685 when mud is a significant component is considered. Specifically the case when the bed is
 686 composed of 25% mud and 75% sand is examined. Equation 4 was evaluated using the same
 687 mean and standard deviations for the mud and sand components as previously, but in this
 688 case the suspended sediment mixture was characterised using, $\theta(z)=0.75-0.05$ in one hundred
 689 equal intervals of 0.0071 between $z=0.01-1.0$ m with 0.01 m spacing. This represents
 690 suspended sediment mass transitioning from 75% sand, 25 % mud at 0.01 m above the bed to
 691 5% sand, 95% mud at 1.0 m above the bed. From this mass size distribution, $P_s^c(a,z)$, the
 692 number size distribution, $P_s^n(a,z)$, was calculated and used to recompute the suspension
 693 acoustic scattering characteristics. For consistency these were combined with the same
 694 profiles of $C(z)$, given in equation (8), used in the previous cases to calculate the
 695 backscattered signal. Following the approach of section 5.5, the inversion was recomputed
 696 with the complete size distribution for the bed, including the muddy and sandy components,
 697 using $P_s^n(a,0.01)$. The outcomes from this scenario are presented in figure 17 and 18.

698



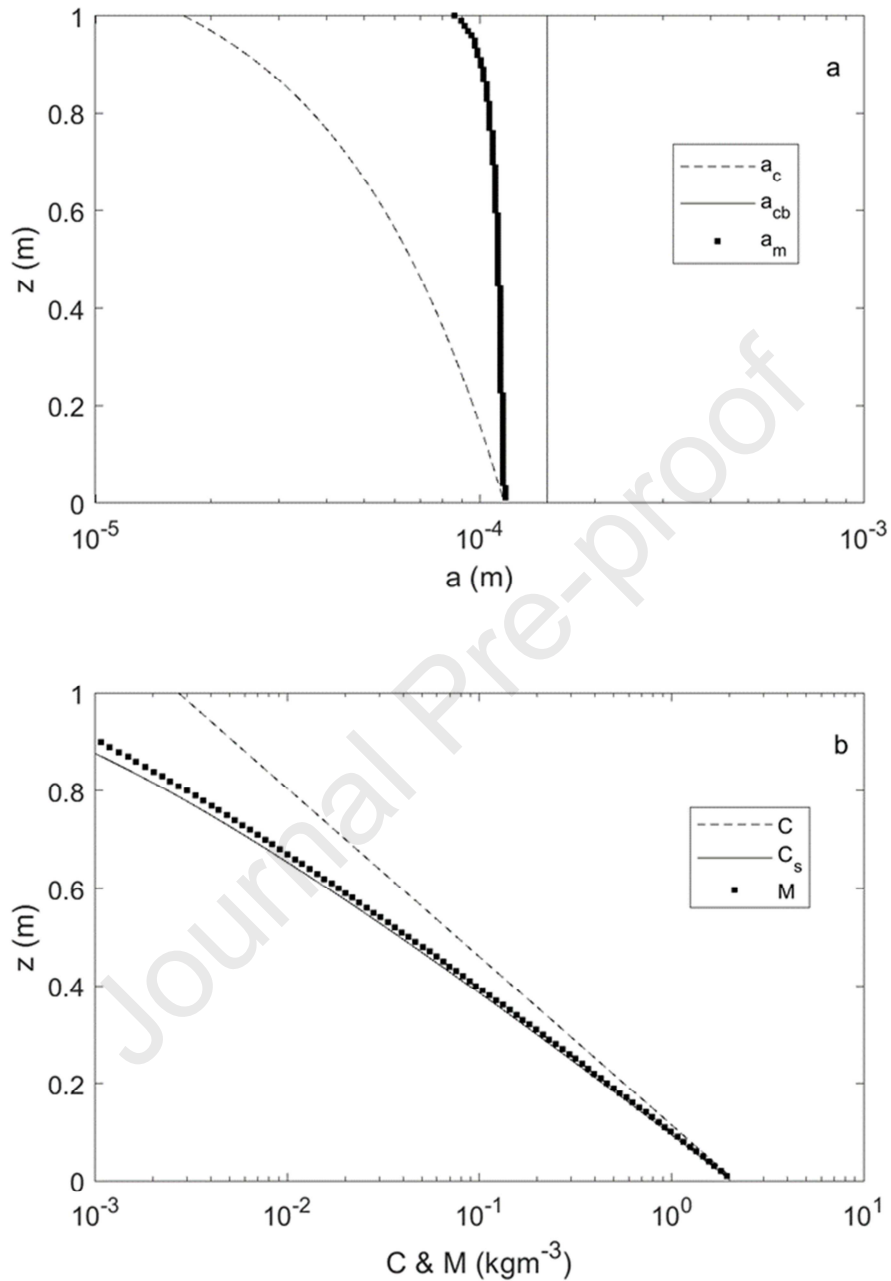
699

700

701 Fig 17. Inversion using $P_s^n(a, 0.01)$ with 25% mud. Comparisons for the Rouse power profile
 702 of a) mean mass radius for the mixed suspended sediments, $a_c(z)$ (---), the sand component
 703 of the bed sediments, a_{cb} (—), and the acoustic inversion $a_m(z)$ (•). b) The concentration for the
 704 mixed suspended sediments, $C(z)$ (---), the sand component of the suspended sediments,
 705 $C_s(z)$ (—), and the acoustic inversion $M(z)$ (•).

706

707



708

709

710 Fig 18. Inversion using $P_s^n(a, 0.01)$ with 25% mud. Comparisons for the exponential profile
 711 of a) mean mass radius for the mixed suspended sediments, $a_c(z)$ (---), the sand component
 712 of the bed sediments, a_{cb} (—), and the acoustic inversion $a_m(z)$ (•). b) The concentration for the
 713 mixed suspended sediments, $C(z)$ (---), the sand component of the suspended sediments,
 714 $C_s(z)$ (—), and the acoustic inversion $M(z)$ (•).

715

716 These figures show that for both the Rouse power law and exponential $C(z)$ profiles the
717 trends for $a_m(z)$ and $M(z)$ are comparable to those in figures 11, 12, 14, 15. The values for
718 $a_m(z)$ are nominally uniform, albeit with mean values smaller than for the two previous
719 scenarios, due to the bed composition having 25% mud content. The profiles for $M(z)$ remain
720 consistently close to the sandy component, $C_s(z)=\theta(z)C(z)$, with height above the bed, as
721 observed in the former two inversions. Therefore, the results from the inversions in sections
722 5.4–5.6 are consistent with $a_m(z)\approx a_{cb}$ and $M(z)\approx C_s(z)$, thereby indicating the generality of the
723 outcomes from this study.

724

725

Journal Pre-proof

726

727

6. Discussion and conclusion

728 The present study was stimulated by measurements of the sediment mass size distribution of
729 the bed and suspended sediments, in an inter-tidal estuarine environment, composed of
730 muddy sand. For the Dee estuary the mud component in the bed sediments was a relatively
731 small fraction of the total mass. Due the hydrodynamic conditions in the estuary, caused by
732 combined waves and tidal flow, significant size sorting of the sediments entrained from the
733 bed into suspension, was measured with height above the bed. It was observed that suspended
734 sediments close to the bed in the estuary were dominated by the sandy component of the
735 surficial sediment layer, while progressively with height above the bed the muddy component
736 became more significant. Analysis of the bed and suspended sediment samples, showed the
737 former could be considered to be reasonably well represented by a lognormal distribution, for
738 the both the mass and number sizes, while for the later, the mass size distribution was bi-
739 modal and the number size distribution was closer to Junge. These contrasting distributions,
740 led to considerations regarding the impact of applying an acoustic inversion, based on a
741 lognormal distribution from bed samples, would have on estimates of $M(z)$ and $a_m(z)$, derived
742 from signals backscattered from a suspension having a distribution closer to Junge.

743

744 Predominately in the literature ABS deployments have been reported as being over sandy
745 sediments, with a unimodal mass sand size distribution, normally represented by a lognormal
746 probability density function (Hay and Sheng, 1992; Crawford and Hay, 1993; Osbourne and
747 Vincent, 1996; Lee et al., 2004; Dolphin and Vincent, 2009; Bolanos et al., 2012; Moate et
748 al., 2016). The source for this representation is usually based on bed samples. The lognormal
749 distribution of the bed samples can be used to theoretically invert the acoustic backscattered
750 data, or, as is often the case, the bed samples can be used to provide a laboratory calibration
751 for the ABS, applicable to the deployment location (Osbourne and Vincent, 1996; Lee et al.,
752 2004; Dolphin and Vincent, 2009). Given the expanding sedimentary environments in which
753 acoustics is being deployed (Best et al., 2010; Sahin et al., 2013; Topping and Wright, 2016;
754 Sahin et al., 2017; Fromant et al., 2017; Vergne et al., 2020), it was considered of value to
755 assess scenarios where the sandy bed sediment size distribution, was used to interpret
756 backscatter data, from a suspension of wide size distribution and with significantly varying
757 sand and mud composition with height above the bed.

758 To carry out the investigation, suspension scenarios were modelled, which reflected some of
 759 the properties identified in the field study. The bed sediments were considered to be primarily
 760 sandy in nature with a lognormal distribution for $P_b^c(a)$ and $P_b^n(a)$. The suspended mass
 761 distribution, $P_s^c(a, z)$, was bi-modal, while the form for $P_s^n(a, z)$ was similar to the Junge
 762 distribution. Two commonly used expressions were applied to represent the suspended
 763 sediment concentration profiles.

764

765 In general, there is little prospect in the marine environment, presently or in the near future,
 766 of being able to obtain detailed high resolution in-situ measurements of $P_s^c(a, z, t)$, where t is
 767 time. There is the LISST instrument, Laser in-situ Scattering and Transmissometry, which
 768 gives relatively coarse measurements of $P_s^c(a, t)$ at a single height above the bed (Agrawal and
 769 Pottsmith, 2000), this can provide a partial solution to the inversion problem. Nevertheless,
 770 the LISST cannot resolve the detailed size distribution of the in-situ suspended sediment
 771 composition with height above the bed, as collected with the multi-tier sampler, and
 772 measured with the Malvern Mastersizer 2000. However, the latter approach only provides
 773 time integrated suspended size distributions, the results of which are shown in figure 3. It is
 774 these limitations in the measurement of profiles of both in-situ $P_s^c(a, z, t)$ and $C(z, t)$ necessary
 775 to assess field inversions of $M(z, t)$ and $a_m(z, t)$, which led to the adoption of the current
 776 modelling approach for the present study, which was both underpinned and stimulated by
 777 actual field observations. As previously noted, invariably it is the dominant sandy component
 778 of the bed sediments collected from the ABS deployment site, which is used for the acoustic
 779 inversion. For the presented scenarios using this approach leads to the results shown in
 780 figures 11 and 12 where essentially the profiles for $a_m(z)$ and $M(z)$ are those of only the sand
 781 component in suspension. Even when the whole particle size distribution of the bed including
 782 both sandy and muddy components is used for the inversion, figures 14 and 15 show some
 783 decrease in mean particle size with height above the bed, however, $a_m(z)$ and $M(z)$ are still
 784 closely aligned with solely the sandy component. Explanations for these responses are
 785 presented in the dominance of the sand scattering component shown in figure 13 and the size
 786 selection and integral ratio calculation of figure 16. Furthermore, increasing the mud content
 787 in the bed to 25%, still yields trends in $a_m(z)$ and $M(z)$ comparable to that of the lower mud
 788 content, that is $a_m(z) \approx a_{cb}$ and $M(z) \approx C_s(z)$. Essentially, for any acoustic inversion based on the
 789 scattering characteristics of the bed sediment size distribution, errors will be introduced into
 790 the acoustic estimates of $C(z)$ and $a_c(z)$ when vertical gradients are present in the suspended

791 size distribution, due to the inappropriate description of the suspension scattering
792 characteristics.

793

794 In the scenarios considered here, there were important changes in the suspended sediment
795 composition with height above the bed, which, if not accurately accounted for, leads to
796 suspended particle size and concentration diverging significantly from what was actually
797 modelled in suspension. Certainly, suspended sediment composition with height above the
798 bed will vary depending on the mud-sand composition of the bed and the hydrodynamic
799 conditions, leading to functional forms for $\theta(z)$ that will vary from the simple linear
800 dependency on z adopted for the scenarios presented here. However, it would seem to be
801 generally the case that suspended sediment size will be overestimated and concentration
802 underestimated, in mixtures of muddy and sandy suspended sediments, when bed samples are
803 used for the inversion of acoustic backscatter signal data. Therefore, acoustic inversions are
804 more problematic for mixed sediments than for the case of unimodal sands and caution needs
805 to be applied in the interpretation of ABS data collected in these more complex sedimentary
806 environments.

807

808 **Acknowledgements**

809 The study was supported by the National Oceanography Centre, UK, the European
810 Commission through the Hydralab contract number 654110 and the NERC, UK, project
811 BLUE-coast, NE/N015894/2. The data were collected as part of the NERC, UK, COHBED
812 field measurements, contract number NE/1027223/1. D. Hurther was supported by the French
813 DGA-funded ANR Astrid Maturation project MESURE (ANR-16-ASMA-0005) The
814 Malvern particle size analysis was carried out at Bangor University with the support of Dr
815 Jaco Baas. Dr Christopher Unsworth of NOC and the formal reviewers are thanked for their
816 critical reading of the manuscript.

817

818

819 **References**

820

821 Agrawal Y.C., and Pottsmith H.C. 2002. Instruments for particle size and settling velocity
822 observations in sediment transport. *Marine Geology*, 168, 89-114.

823

824 Babin, M., Morel, A., Fournier-Sicre, V., Fell, F., Stramski, D. 2003. Light scattering
825 properties of marine particles in coastal and open ocean waters as related to the particle mass
826 concentration. *Limnol. Oceanogr.*, 48(2), 2003, 843–859.

827

828 Bartholoma, A., A. Kubicki, Badewien T. H. and Flemming B. W. 2009. Suspended
829 sediment transport in the German Wadden Sea—Seasonal variations and extreme events,
830 *Ocean Dyn.*, 59(2), 213–225.

831

832 Best J., Simmons S., Parsons D., Oberg K., Czuba J., and Malzone C. 2010. A new
833 methodology for the quantitative visualization of coherent flow structures in alluvial channels
834 using multibeam echo sounding (MBES). *Geophysical Research Letters*, 37, L06405

835

836 Betteridge, K.F.E., Thorne, P.D. and Cooke, R.D., 2008. Calibrating multi-frequency
837 acoustic backscatter systems for studying near-bed suspended sediment transport processes.
838 *Continental Shelf Research.*, 28, 227-235.

839

840 Bolanos R, Thorne PD and Wolf J. 2012. Comparison of measurements and models of bed
841 stress, bedforms and suspended sediments under combined currents and waves. *Coastal*
842 *Engineering* 62, 19-30.

843

844 Brand E., Chen M. and Montreuil A. 2020. Optimizing measurements of sediment transport
845 in the intertidal zone. *Earth-Science Reviews*, 200, 103029, 1-10.

846

847 Buonassissi, C.J. and Dierssen, H.M. 2010. A regional comparison of particle size
848 distributions and the power law approximation in oceanic and estuarine surface waters, *J.*
849 *Geophys. Res.*, 115, C10028, doi:10.1029/2010JC006256.

850

- 851 Cacchione D. A., Thorne P. D., Agrawal Y. and Nidzieko N. J. 2008. Time averaged near-
852 bed suspended sediment concentrations under waves and currents; comparison of measured
853 and model estimates. *Continental Shelf Research*, 28, 470-484.
- 854
- 855 Cheng C., Song Z., Wang Y. and Zhang J. 2013. Parameterized expressions for an improved
856 Rouse equation. *International Journal of Sediment Research* 28 523-534.
- 857
- 858 Crawford, A.M., Hay, A.E., 1993. Determining suspended sand size and concentration from
859 multifrequency acoustic backscatter. *J. Acoust. Soc. Am.* 94(6), 3312-3324.
- 860
- 861 Dolphin, T and Vincent C. 2009. The influence of bed forms on reference concentration and
862 suspension under waves and currents. *Continental Shelf Research* 28, 424-432.
- 863
- 864 Dwinovantyo A., Manik H M, Prartono T., Susilohadi and Ilahude D. 2017. Estimation of
865 suspended sediment concentration from Acoustic Doppler Current Profiler (ADCP)
866 instrument: A case study of Lembah Strait, North Sulawesi. *IOP Conf. Series: Earth and
867 Environmental Science* 54 (2017) 012082 doi:10.1088/1755-1315/54/1/012082.
- 868
- 869 Flammer G. H. 1962. Ultrasonic measurements of suspended sediments. *Geological Survey
870 Bulletin No 1141-A*, United States Government Printing Office, Washington.
- 871
- 872 Fromant G., Floch F., Lebourges-Dhaussy A., Jourdin F., Perrot Y., Le Dantec N. and
873 Delacourt C. 2017. In Situ Quantification of the Suspended Load of Estuarine Aggregates
874 from Multifrequency Acoustic Inversions. *Journal of Atmospheric and Oceanic Technology*,
875 34, 1625-1643.
- 876
- 877 Green M.O. and Black K.P 1999. Suspended-sediment reference concentration under waves:
878 field observations and critical analysis of two predictive models. *Coastal Engineering*, 38,
879 115-141.
- 880
- 881 Guerrero, M., Szupiany, R. N. and Latosinski, F. 2013. Multi-frequency acoustics for
882 suspended sediment studies: an application in the Parana River. *Journal of Hydraulic
883 Research*, 51 (6), 696–707.

- 884 Hanes, D.M., Vincent, C.E., Huntley, D.A., and Clarke, T.L., 1988. Acoustic measurements
885 of suspended sand concentration in the C2S2 experiment at Stanhope Land, Prince Edwards
886 Island, *Marine Geol.* 81, 185-196.
- 887
- 888 Hanes, D.M., 1991. Suspension of sand due to wave groups, *Journal of Geophysical*
889 *Research*, Vol. 96(C5), 8911-8915.
- 890
- 891 Hay, A.E. and Mercer, D.G. 1985. On the theory of sound scattering and viscous absorption
892 in aqueous suspensions at medium and short wavelengths. *J. Acoust. Soc. Am.* 78(5) 1761-
893 1771
- 894 Hay A. E. 1991. Sound scattering from a particle-laden turbulent jet, *J. Acoust Soc. Am.*, 90,
895 2055-2074.
- 896
- 897 Hay, A.E. and Sheng. J., 1992. Vertical profiles of suspended sand concentration and size
898 from multifrequency acoustic backscatter. *J. Geophys. Res.* 97(C10). 15661-15677.
- 899
- 900 He C and Hay A. E. 1993. Broadband measurements of the acoustic scattering cross section
901 of sand particles in suspension. *J. Acoust. Soc. Am.* 94(4) 2247-2254.
- 902
- 903 Holdaway, G.P. Thorne, P.D., Flatt, D., Jones, S.E., Prandle, D. 1999. Comparison between
904 ADCP and transmissometer measurements of suspended sediment concentration. *Continental*
905 *Shelf Research* 19 421-441.
- 906
- 907 Junge, C. E. 1963. Sulfer in the Atmosphere. *J. Geophys. Res.*, Vol 68, No 13, 3975-3976.
- 908
- 909 Kostadinov, T.S., Siegel, D.A., Maritorena, S. (2009), Retrieval of the particle size
910 distribution from satellite ocean color observations, *J. Geophys. Res.*, 114, C09015,
911 doi:10.1029/2009JC005303.
- 912
- 913 Lichtman, I. D., Baas, J. H., Amoudry, L. O., Thorne, P. D., Malarkey, J., Hope, J. A.,
914 Peakall, J., Paterson, D. M., Bass, S. J., Cooke, R. D., Manning, A. J., Davies, A. G.,
915 Parsons, D. R., Ye, L. 2018 Bedform migration in a mixed sand and cohesive clay intertidal
916 environment and implications for bed material transport predictions. *Geomorphology*, 315,
917 17-32.

918

919 Lee, G., Dade, W.B., Friedrichs, C.T., and Vincent, C.E., 2004. Examination of reference
920 concentration under waves and currents on the inner shelf. *J. Geophys. Res.* 109. C02021.

921

922 Libicki, C., Bedford, K.W., and Lynch, J.F., 1989. The interpretation and evaluation of a 3-
923 MHz acoustic backscatter device for measuring benthic boundary layer sediment dynamics.
924 *Journal of the Acoustical Society of America*, 85 (4): 1501-1511.

925

926 Lynch, J.F., Gross, T.F., Brumley, B.H. and Filyo, R.A., 1991. Sediment concentration in
927 HEBBLE using a 1-MHz acoustic backscatter system, *Marine Geology*, 99, 361-385.

928

929 Lynch, J.F., Irish, J.D., Sherwood, C., Agrawal, Y.C., 1994. Determining suspended
930 sediment particle size information from acoustical and optical backscatter measurements,
931 *Continental Shelf Research*, Vol. 14(10/11), 1139-1165.

932

933 MacDonald IT, Vincent CE, Thorne PD and Moate PD. 2013. Acoustic scattering from a
934 suspension of flocculated sediments. *J. Geophysical Research: Oceans*, Vol 118, 1-14.

935

936 Moate B. D. and Thorne P. D. 2009. Measurements and inversion of acoustic scattering from
937 suspensions having broad size distributions. *J. Acoust. Soc. Amer.* Vol 126(6), 2905-1917.

938

939 Moate BD and Thorne PD. 2012. Interpreting acoustic backscatter from suspended sediments
940 of different and mixed mineralogical composition. *Continental Shelf Research*, 46, 67-82.

941

942 Moate B. D., Thorne P. D. and Cooke R. D. 2016. Field deployment and evaluation of a
943 prototype autonomous two dimensional acoustic backscatter instrument: The Bedform And
944 Suspended sediment Imager (BASSI). *Continental Shelf Research* 112 78-91.

945

946 Moore, S.A., and Hay, A.E., 2009. Angular scattering of sound from solid particles in
947 turbulent suspension. *J. Acoust. Soc. Am.*, 126 (3), 1046-1056.

948

949 Moore, S. A., Le Coz J., Hurther D. and Paquier A. 2012. On the application of horizontal
950 ADCPs to suspended sediment transport surveys in rivers. *Continental Shelf Research*, 46,
951 50-63.

952

953 Moore, S. A., Le Coz J., Hurther D. and Paquier A. 2013. Using multi-frequency acoustic
954 attenuation to monitor grain size and concentration of suspended sediment in rivers. *Journal*
955 *Acoustical Society America*, 133(4), 1959-1970.

956

957 Nielsen P. 1992. *Coastal Bottom Boundary Layers and Sediment Transport*. Advanced series
958 on ocean engineering, volume 4. World Scientific, Singapore, 324 pp.

959

960 O'Hara Murray R. B., Thorne P. D. and Hodgson D. M. 2011, Intrawave observations of
961 sediment entrainment processes above sand ripples under irregular waves. *JGR*,116, doi:
962 10.1029/2010JC006216.

963

964 Osbourne P.D. and Vincent C.E., 1996 Vertical and horizontal structure in suspended sand
965 concentration and wave-induced fluxes over bedforms. *Mar Geo.*, 115, 207-226.

966

967 Richards S.D., Leighton T.G. and Brown N.R., 2003. Visco-inertial absorption in dilute
968 suspensions of irregular particles. *Proceedings of the Royal Society London*, 459, 2153-2167.

969

970 Rose, C.P. and Thorne, P. D. 2001. Measurements of suspended sediment transport
971 parameters in a tidal estuary. *Continental and Shelf Research*. (21) 1551-1575.

972

973 Rouse, H. 1937. Modern conceptions of the mechanics of turbulence: *American Society of*
974 *Civil Engineers, Transactions*, v. 102, p. 436-505

975

976 Sahin C., Safak I., Hsu T., and Sheremet A. 2013. Observations of suspended sediment
977 stratification from acoustic backscatter in muddy environments. *Marine Geology*, 336, 24–32.

978

979 Sahin C., Verney R., Sheremet A., and Voulgaris G. 2017. Acoustic backscatter by
980 suspended cohesive sediments: Field observations, Seine Estuary, France. *Continental Shelf*
981 *Research*, 134, 39-54

982

983 Sassi, M. G., Hoitink A. J. F. and Vermeulen B. 2012. Impact of sound attenuation by
984 suspended sediment on ADCP backscatter calibrations, *Water Resour. Res.*, 48, W09520,
985 doi:10.1029/2012WR012008.

- 986
- 987 Sassi, M. G., Hoitink, A. J. F. Vermeulen, B. and Hidayat, H. 2013. Sediment discharge
988 division at two tidally influenced river bifurcations, *Water Resources Research*, 49 (4), 2119–
989 2134.
- 990
- 991 Schaafsma A. S. and Hay A. E. 1997. Attenuation in suspensions of irregularly shaped
992 sediment particles: A two-parameter equivalent spherical scatterer model. *J. Acoust. Soc.*
993 *Am.* 102, 1485-1502.
- 994
- 995 Schmidt, W., 1925. *Der Massenaustausch in freier Luft und verwandte Erscheinungen,*
996 *Probleme der kosmischen Physik*, Bd. 7, viii, 118 p. (H. Grand, Hamburg 1925).
- 997
- 998 Sheng, J. and Hay A. E. 1988. An examination of the spherical scatterer approximation in
999 aqueous suspensions of sand. *J. Acoust. Soc. Am.* 83, 598-610.
- 1000
- 1001 Sheng, J., Hay, A.E., 1995. Sediment eddy diffusivities in the nearshore zone, from
1002 multifrequency acoustic backscatter, *Continental Shelf Research*, Vol. 15(2/3), 129-147.
- 1003
- 1004 Shi Z., Ren L. F. and Lin H. L. 1996. Vertical suspension profiles in the Changjiang estuary.
1005 *Marine Geology*, 130, 29-37.
- 1006
- 1007 Shi Z., Ren L. F., Zhang S. Y. and Chen J. Y. 1997. Acoustic imaging of cohesive sediment
1008 resuspension and re-entrainment in the Chanjiang estuary, East China Sea. *Geo-marine*
1009 *Letters*, 17, 162-168.
- 1010
- 1011 Soulsby R. L. 1997 *Dynamics of marine sands.* Thomas Telford publication, UK. 249 pp.
- 1012
- 1013 Souza, A. J., L. Alvarez G and Dickey T. D. 2004. Tidally induced turbulence and suspended
1014 sediment, *Geophys. Res. Lett.*, 31, L20309, doi:10.1029/2004GL021186.
- 1015
- 1016 Thorne, P.D., Hardcastle, P.J. & Soulsby, R.L. 1993. Analysis of acoustic measurements of
1017 suspended sediments. *Journal of Geophysical Research*, 98, 899 910.
- 1018

- 1019 Thorne, P.D., Hardcastle, P.J., 1997. Acoustic measurements of suspended sediments in
1020 turbulent currents and comparison with in-situ samples. *Journal of the Acoustical Society of*
1021 *America* 101 (5) (Pt. 1), 2603-2614.
- 1022
- 1023 Thorne, P. D. Williams, J. J. and Davies, A. G. 2002. Suspended sediments under waves
1024 measured in a large-scale flume facility. *J. Geophysical Research*. Vol 107, No C8, 4.1-4.16.
- 1025
- 1026 Thorne P. D. and Buckingham M. J. 2004. Measurements of scattering by suspensions of
1027 irregularly shaped sand particles and comparison with a single parameter modified sphere
1028 model. *J. Acoust Soc Amer.* 116 (5) 2876-2889.
- 1029
- 1030 Thorne P. D. and Meral R. 2008. Formulations for the scattering properties of sandy
1031 sediments for use in the application of acoustics to sediment transport. *Continental Shelf*
1032 *Research*, 28, 309-317.
- 1033
- 1034 Thorne P.D. and Hurther D. 2014. An Overview on the use of backscattered sound for
1035 measuring suspended particle size and concentration profiles in non-cohesive inorganic
1036 sediment transport studies. *Continental Shelf Research*. 73, 97-118.
- 1037
- 1038 Thorne P.D., MacDonald I.T. and Vincent C.E. 2014. Modelling acoustic scattering by
1039 suspended flocculating sediments. *Continent Shelf Research* 88, 81-91.
- 1040
- 1041 Thorne P.D., Hurther D., Cooke R.D., Caceres I., Barraud P.A. and Sánchez-Arcilla A. 2018.
1042 Developments in acoustics for studying wave-driven boundary layer flow and sediment
1043 dynamics over rippled sand-beds. *Continental Shelf Research*, 166, 119-137.
- 1044
- 1045 Topping, D.J., and Wright, S.A., 2016, Long-term continuous acoustical suspended-sediment
1046 measurements in rivers—Theory, application, bias, and error: U.S. Geological Survey
1047 Professional Paper 1823, 98 p., <http://dx.doi.org/10.3133/pp1823>.
- 1048
- 1049 Urlick R.J, 1948. The absorption of sound in suspensions of irregular particles. *J. Acoust Soc.*
1050 *Am.* 20, 3, 283-289.
- 1051

- 1052 van der Werf, J.J., Ribberink, J.S., O'Donoghue, T., Doucette, J.S., 2006. Modelling and
1053 measurement of sand transport processes over full-scale ripples in oscillatory flow. *Coast.*
1054 *Eng.* 53 (2006), 657–673.
1055
- 1056 Vergne, A., LeCoz, J., Berni, C. and Pierrefeu, G. 2020. Using a down-looking
1057 multifrequency acoustic backscatter system (ABS) for measuring suspended sediments in
1058 rivers. *Water Resources Research*, 56, e2019WR024877.
1059 <https://doi.org/10.1029/2019WR024877>
1060
- 1061 Vincent, C. E., Young, R. A. and Swift, D. J. P. 1982. On the relationship between bedload
1062 and suspended transport on the inner shelf, Long Island, New York. *Journal of Geophysical*
1063 *Research* Vol 87(C6) 4163-4170.
1064
- 1065 Villard P. V., Osborne P. D. and Vincent C.E. 2000. Influence of wave groups on SSC
1066 patterns over vortex ripple. *Continental Shelf research* 20, 2391-2410.
1067
- 1068 Vincent, C.E., Green, M.O., 1990. Field measurements of the suspended sand concentration
1069 profiles and fluxes and of the resuspension coefficient γ_0 over a rippled bed, *Journal of*
1070 *Geophysical Research*, Vol. 95(C7), 11,591-11,601.
1071
- 1072 Whitehouse, R.J.S., Soulsby, R.L., Roberts, W. and Mitchener, H.J. 2002. Dynamics of
1073 estuarine muds. Technical Thomas Telford publication, UK. 210 pp.
1074
- 1075 Young, R.A., Merrill, J.T., Clarke, T.L., and Proni, J.R., 1982. Acoustic profiling of
1076 suspended sediments in the marine bottom boundary layer. *Geophysical Research Letters*, 9
1077 (3): 175-188.
1078

Highlights

A numerical study explores the acoustic backscatter from a suspension of a mud-sand mixture with a composition varying with height above the bed.

Changes in the mud-sand composition with height above the bed generally leads to errors in the acoustic estimates of particle size and concentration.

When using bed samples, the dominant sand component is generally chosen for the acoustic inversion, leading to an overestimate of mean suspended sediment size and an underestimate of the concentration.

Obtaining accurate measurements of suspended sediments acoustically in a mixed mud-sand environment can be problematic

No conflict of interest has been declared by the author(s).”

Journal Pre-proof

Declaration of interests

The authors declare that they have no known competing financial interests or personal relationships that could have appeared to influence the work reported in this paper.

The authors declare the following financial interests/personal relationships which may be considered as potential competing interests:

Journal Pre-proof